Targeted Sequence Delivery Platform with ROS-Response for the Treatment of Osteoarthritis

Doroteja Bednjanec

Master's thesis

Åbo Akademi University
26.05.2021.

Masters' degree of Biomedical Imaging

Pharmaceutical Sciences Laboratory
Faculty of Science and Engineering
Åbo Akademi University and Turku Bioscience center, University of Turku and Åbo Akademi University

Credits: 20 ECTS

Supervisor:
Associate Prof. Hongbo Zhang

Passed:

Grade:

Abstract

Åbo Akademi University
Master's Degree Programme in Biomedical Imaging
Faculty of Science and Engineering

DOROTEJA BEDNJANEC:

Targeted Sequence Delivery Platform with ROS- Response for the Treatment of Osteoarthritis

Master's thesis, 55 pp.
Faculty of Science and Engineering
May, 2021

Arthritis is a common problem affecting elderly people today. One specific form of arthritis is osteoarthritis, caused by lubrication deficiency at the joint surface. Due to genetics, aging, stress factors, or accidents, the cartilage layer breaks down causing inflammation of the joint. When no cartilage surrounds the bone, neighboring bones scratch each other and cause pain. To prevent and slow down those events, nanomedicine has become a popular field of study and research. The main objective of this research was to develop targeted drug delivery method for treating osteoarthritis using, small nano- and micro- compositions. Another important objective was to find a way for the composition with the lubricated surface, to target damaged tissue. The core of the built nanoparticle was Cerium oxide (CeO_2), surrounded by a mesoporous silica nanoparticle (MSN) shell. Using microfluidics, the drug Agomir874 was loaded within core-shell nanoparticles, and then surrounded by the PEO-b-PFMA microparticles. The polymer contained collagen IgG2, for antibody-antigen binding to improve the elasticity of the joint. Finally, the drug 5-ASA was inserted within polymer in order to reduce inflammation in the damaged tissue. As the PEO-b-PFMA particles were diluted, the right solvent was needed to be found in order for the polymer particles to stay stable. In the future, with the help of different imaging techniques, it will be possible to determine how much drug is loaded within the particle and whether the drug loading of the particles is successful.

KEYWORDS: Cartilage, Chip, Drug delivery, Nanoparticle, Microfluidic device, Polymer

ABBREVIATIONS

$AgNO_3$	Nitric acid
Au NR's	Gold Nanorods
$Ce(NO_3)_3$	Cerium Nitrate
CeO_2 NP	Cerium Oxide nanoparticle
CH_2Cl_2	Dichloromethane
cm^3/g	Centimeter cubed per gram
CTAB	Cetyl trimethylammonium bromide
ECM	Etracellular matrix
Etax	Ethanol
g	gram
$HAuCl_4$	Chloroauric acid
$HC_6H_7O_6$	Ascorbic acid
HCl	Hydrochloric acid
mol	mole
nmol	nanomol
mg	milligram
mg/mL	milligrams per milliliter
mL	milliliter
mL/h	milliliter per hour
mmol	mili mols per liter
MSN	Mesoporius silica nanoparticle
$NaBH_4$	Sodium Borohydride
NIR	near-infrared
nm	nanometer
nm^2	square nanometer
OA	OsteoarthritisF
PEO	Poly (ethylene oxide)
PEO-b-PFMA	Poly(ethylene oxide)-b-poly(furfuryl methacrylate)
PH	Potential of Hydrogen
Pluronic F127	poly(ethylene oxide)-poly(propylene oxide)-poly(ethylene oxide) triblock copolymer

ROS	reactive oxygen species
RPM	revolutions per minute
SEM	scanning electron microscope
TEM	transmission electron microscope
TEOS	Tetraethyl orthosilicate
μL	microliters
5-ASA	5-aminosaliclic acid
^{o}C	Celsius

Contents

1 INTRODUCTION

Osteoarthritis is a common condition impacting millions of people worldwide (Wittenauer et al., 2013). This occurs when there is a lubrication deficiency of the joint surface, causing cartilage breakdown which leads to pain and movement limitation at the joint. As science has progressed, nanomedicine has become a popular field of research, as it provides the potential for new ways to treat and prevent diseases such as osteoarthritis. This can be done by using micro- and nano-composites to develop targeted drug delivery methods. This project focused on developing a specific drug delivery system at the nanoscopic scale for treating osteoarthritis.

Each micro- and nano- composites were chosen for the specific task, and to be able to perform as unity, without damaging the living cells and to reduce the pain and inflammation for the treatment of osteoarthritis. Figure 1 explains the building blocks of the composites in the project, as well as their geometric location.

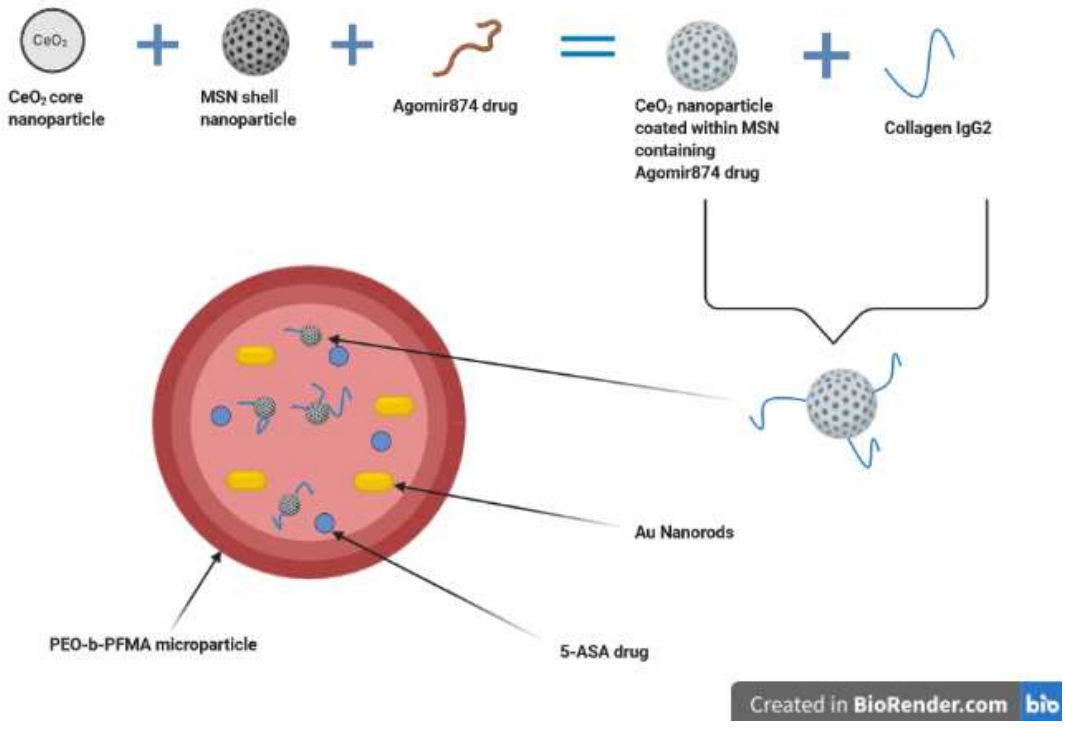

Figure 1. This is a brief overview of the drug delivery system designed for this project. The first drug, Agomir874, is inserted to the CeO_2 within MSN nanoparticles, which are comprised of CeO_2 core and MSN shell. These CeO_2 within MSN nanoparticles were then coated with PEO-b-PFMA microparticles, known

also as the polymer, for lubrication. Within this polymer, Au nanorods and 5-ASA drug were inserted. Collagen IgG2 was attached to the CeO_2 within the MSN nanoparticles, to bind with collagen from the joints (Created with BioRender.com).

Cerium oxide nanoparticles (CeO_2 NP`s) were the core of the particle, surrounded with the mesoporous silica shell (MSN). The CeO_2 core was chosen in order to reduce the inflammation, while the MSN shell due to regeneration and easy manipulated surface (Hosseini and Mozafari, 2020). Within core and shell, the drug Agomir874 was loaded.

This specific drug was chosen due to possibility to mimic miRNA function to regulate gene expression of wanted genes. Agomir874 was a perfect candidate because of the good stability and the possibility to penetrate the cell membrane barriers to reach the target (Catalanotto et al., 2016).

The nanocomposites were coated within the Poly (ethylene oxide)-b-poly (furfuryl methacrylate) (PEO-b-PFMA) microparticles. This polymer makes the surface of the drug delivery particle smooth and lubricated, to prevent tissue damage. The PEO-b-PFMA responds to the reactive oxygen species (ROS), found in inflamed joint part, to make targeting possible. Finally, it releases the drug with near-infrared light exposure (Salma et al., 2018).

Within the PEO-b-PFMA microparticles, collagen IgG2 was attached to the surface of the CeO_2 coated with the MSN nanoparticles to form antibody-antigen binding to the main component in the cartilage, collagen II to improve elasticity of the joint.

Beside CeO_2 within MSN found within PEO-b-PFMA microparticles, there was another component coated, 5-aminosalicylic acid (5-ASA). This drug is usually used to treat inflammatory diseases and healing the damaged tissue. It is chemically related to aspirin and it stimulates different nuclear receptors which are responsible for control of the inflammation and cell development (Perrotta et al., 2015).

For the photothermal responsive imaging purposes, gold nanorods (Au nanorods), were coated within polymer as well. Au nanorods have good biocompatibility, low toxicity, and controllable surface chemical properties (Haine and Niidome, 2017). The photothermal effect of the nanorods plays an important role in information recording.

As described above, the particles built supposed to have mentioned functions and the exact position within polymer.

2 LITERATURE REVIEW

2.1 Background and Significance

Osteoarthritis (OA), also called a joint disease, is a common problem today associated with aging. OA is a type of disease that affects joint cartilage, causing neighboring bones to rub simultaneously. This result in inflammation of joint and surrounded tissue, which causes pain, stiffness, and difficulties performing any kind of movement (Loscalzo, 2011). This chronic disease can affect all joints, ranging from the smaller ones, such as joints in fingers, to the bigger ones, such as hip and spine joints. OA mostly occurs in the older population, but due to trauma, injury, diabetes, obesity, or genetic predisposition, it can also affect younger patients (Blagojevic et al., 2010). While OA is more common in women, around 15% of all adults over 60 years of age carry some level of the disease. The United Nations, predicted around 130 million people will deteriorate from OA in next 30 years (WHO, 2013).

To prevent and reduce the symptoms of OA, medications and surgeries are necessary. It is possible to reduce the symptoms by exercising if the OA is showing light symptoms if movement in the joint is not limited or painful (Hunter and Eckstein, 2009). However, as age increases, exercise often becomes limited, and the only treatment options are medications or surgery. For this reason, OA remains a common topic of different research projects. If the patient seeks medical help for limited and painful movements, it will be examined with an MRI scan and X-ray, however, it can still be difficult to distinguish weather a patient has the disease or not. If the specialist determines that the patient has the disease, then the patient can be treated with medications to prevent the pain, but if the case is more critical, surgery is needed. While, there are options available to reduce the symptoms, there is still no product that can completely cure or prevent OA (Grässel and Muschter, 2020).

In order to advance the monitoring of the OA and improve treatment options, the development of medications to reverse the progression of the disease will be necessary. The following project was planned, and this specific design was selected because of the intra-articular drug delivery proven to be the most useful from the previous research. But, for the system to be therapeutic, the efficiency of the drug delivery system is crucial. Due

to that reason, for this therapy, synthesis of a complicated system is necessary (Singh and Lillard, 2009).

2.2 Osteoarthritis (OA)

The most frequent form of arthritis is osteoarthritis (OA). It is a joint disease affecting around 250 million people in the world (Mora et al., 2018b). This disease mainly affects the elderly; however it can affect young people as well, due to certain preexisting conditions, such as obesity and diabetes. Other stress factors causing OA are shock factors due to injury, continuing to perform everyday activities before the recovery of the injury, etc. Due to an increase in obesity and diabetes cases in the world, the number of osteoarthritis cases rises simultaneously, and the number will continue to rise in the future (Wittenauer et al., 2013).

Joints are comprised of many parts including cartilage, bones, ligaments, and a synovial membrane. When there is not enough lubrication in the joint, the movement of the joint becomes limited and painful, which are the signs of OA.

OA can be divided into two groups based on the cause; non-traumatic (primary), and traumatic (secondary). It is proven today that OA is caused by factors such as inflammation, trauma, biochemical reactions, and mechanical forces. In the early stage of the disease, as cartilage is not capable of producing pain or inflammation, pain comes from changes in the non-cartilage part of the joint. As the disease proceeds, the cartilage is affected, as well as the entire joint, and changes occur in the form of bone remodeling, muscle dystrophy, and other adverse effects shown in the figure 2 (Mora et al., 2018a).

As the disease progresses, the inflammation can be divided into chronic and low-grade inflammation. In the early stages of the disease, the aggression of inflammatory cells into synovium, known as synovitis, is found. Then, synovial fluid inflammatory mediators are established, such as plasma proteins, leukotrienes, cytokines, growth factors, nitric oxide, and complement components. All of these factors result in cartilage breakdown and collagen demolition (Mora et al., 2018a).

Another factor involved in the progression of OA are white blood cells. In the animal models, it was proven that macrophages were connected with the process of forming the OA (Mora et al., 2018a) . Certain molecules released as part of a protective mechanism during the extracellular matrix (ECM) division are acknowledged by the inherent immune cells, leading to tissue demolition.

With various factors contributing to the progression of OA, it is important to find a suitable, non-surgical treatment of the disease. Despite OA being one of the most studied diseases in research, it still does not have the most effective treatment. The therapy for early-stage OA is exercise, which is recommended by the medical expertise. Exercise helps to delay the disease progression, but it does not cure or reverse it (Mora et al., 2018a).

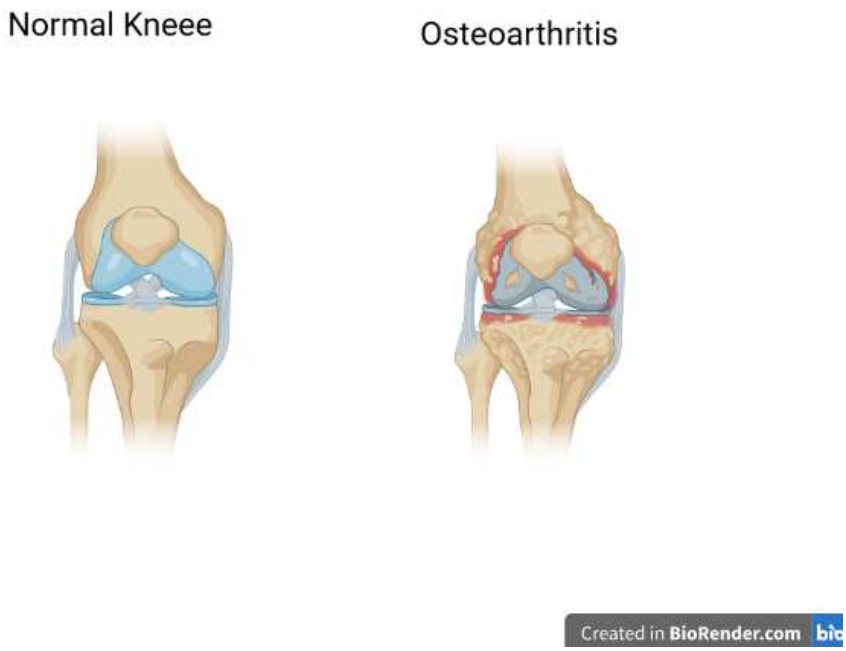

Figure 2. Changes occurring in form of bone remodeling , as progression of OA. Figure shows a healthy knee joint to the left, and a knee joint with osteoarthritis to the right, where loss of cartilage is present (Created with BioRender.com)

2.3 Cartilage

To treat OA, it is important to understand the biology and functions of cartilage first. There are different types of cartilage in the human body; elastic, hyaline, and fibrocartilaginous cartilage (Naumann et al., 2002). The differentiation comes from their molecular structure.

The primary form of cartilage is hyaline cartilage. As part of the hyaline cartilage group, articular cartilage is divided into four zones; the superficial, transitional, radial, and calcified zones. In the calcified zone, cartilage is in a coalition with a bone. These zones differentiate by the organization of the collagen network, as well as in the amount and type of proteoglycans (Mora et al., 2018a).

Type II collagen is the main compound of healthy articular cartilage. The main proteoglycan present in the cartilage is aggrecan, but some other proteoglycans present in cartilage include syndecans, glypican, decorin, and biglycan (Wittenauer et al., 2013).

Endochondral ossification is a process of creating a bone tissue with the presence of cartilage. It occurs during development and bone healing. This process occurs during development of the articular cartilage, and takes place through four steps (Mackie et al., 2008). The first step includes chondrogenesis differentiation and mesenchymal condensations, where mesenchymal chondroprogenitor cells separate into chondrocytes and the chondroitin tissues. Then, the differentiation of chondrocytes and hypertrophy occurs. This differentiation is essential in cartilage formation. It plays an important role after the cartilage is replaced by the bone, where chondrocytes continue to separate. The final two steps are mineralization of the matrix and formation of bone (Umlauf et al., 2010).

During bone formation, blood vessels occupy the cartilage, starting from the perichondrium. Hypertrophic chondrocytes start to mineralize the extracellular matrix of the perichondrum. The development of the definitive bone matrix is possible with the help of mineralizing osteoblasts and osteoclasts that move into the remodeling cartilage (Umlauf et al., 2010).

Specific development roles of the cartilage are still poorly understood. However, endochondral ossification and chondrocyte differentiation play the main role in have been mostly studied cartilage development. The connection between osteoarthritis and cartilage development has been studied, as it is believed that similar processes are involved at the beginning and progression of the OA (Mackie et al., 2008).

2.4 Mesoporous silica nanoparticles (MSN)

Particles varying in size between 10 nm and 1000 nm are called nanoparticles. They can be used as drug carriers, where they are loaded with drugs or antigens and release them at specific location under specific conditions. They are perfect for drug delivery because they control release of the drug to the targeted area. NPs, are often coated with a polymer, to improve the delivery and reduce side effects (Mohanraj and Chen, 2006).

The most commonly used nanoparticle is mesoporous silica nanoparticle (MSN). In the last decade, MSN gained attention for its possibility to adjust and control its chemical and

physical properties. As it contains hundreds of empty channels, MSN appears to have porous surface. As shown in figure 3, MSN has a high surface area and suitable pore-volume ratio, making it a perfect candidate for drug delivery. A drug can be easily encapsulated in the nanoparticle, while the size of the particle is strictly controlled. MSN contains silanol (Si-OH) in high amounts on its surface, which allows MSN to attract different polar molecules. This ability is important because the attracted polar molecules can change surface properties of MSN and its application in drug delivery (Douroumis et al., 2013).

Particle size and distribution are important characteristics in drug delivery compositions. The goal is to control the nanoparticle properties and drug release to achieve better results. An important factor for controlling drug release is pore size. The pore size controls the absorption of molecules in MSN matrix by selectively loading drug molecules, which precisely shows the amount of the drug released. The pore size can vary from 2-10 nm and can be adjusted by changing the surface chain length (Al-snafi, 2014). As the MSN pore size is uniform and adjustable, this allows for molecules of various sizes to be absorbed. The release and drug loading kinetics of different pore sizes showed the impact of the pore sizes on drug release. For an example, different pH- sensitive gatekeepers were able to release the drug only in the targeted site, not affecting the healthy cells, where smaller molecules of MSN were able to stay longer in the blood circulation, and transfer faster comparing to larger molecules. (Douroumis et al., 2013).

The pore surface of MSN controls the dosage of the drug within MSN matrix. Surface area plays a critical role in drug delivery; larger surface areas, lead to higher drug absorption within the matrix of MSN. By modifying the surface of MSN it is possible to increase or decrease the surface area, thereby adjusting the drug dosage and release (Jafari et al., 2019).

The pore volume on the surface of MSN controls drug loading. The volume varies from 0.9 cm^3/g to 2/0 cm^3/g. High drug amounts absorbed into the MSN matrix indicate a larger pore volume. There are interactions with drug molecules and the pore surface as well as molecules within MSN matrix. Connections within molecules can be weak and lead to guest molecules to enter the matrix, which could lead to unwanted molecules within MSN, taking the space for the wanted drug loading. To prevent the guest molecules from

entering, it is important to control the pore volume to indicate the drug amount absorbed (Douroumis et al., 2013).

Nanoparticles are prepared from various materials, such as proteins or polymers. It is important to use non-toxic materials when developing drug delivery systems. MSN has been proven to be very biocompatible and non-toxic in humans (Douroumis et al., 2013).

The preparation of MSN depends on desired size, delivery of the drug, surface characteristics, and biodegradability. MSN is a stable nanoparticle, with excellent thermal and chemical properties. Both the inside and outside of the particle are easily controlled to fit necessary expectations for the desired drug (Zhou et al., 2018).

Monitoring drug release from MSN systems is done with the help of fluorescein dyes, such as fluorescein, Texas red, and rhodamine B. These guest molecules control the gate-opening trigger which decides when and how much drug will be released to living cells (Douroumis et al., 2013).

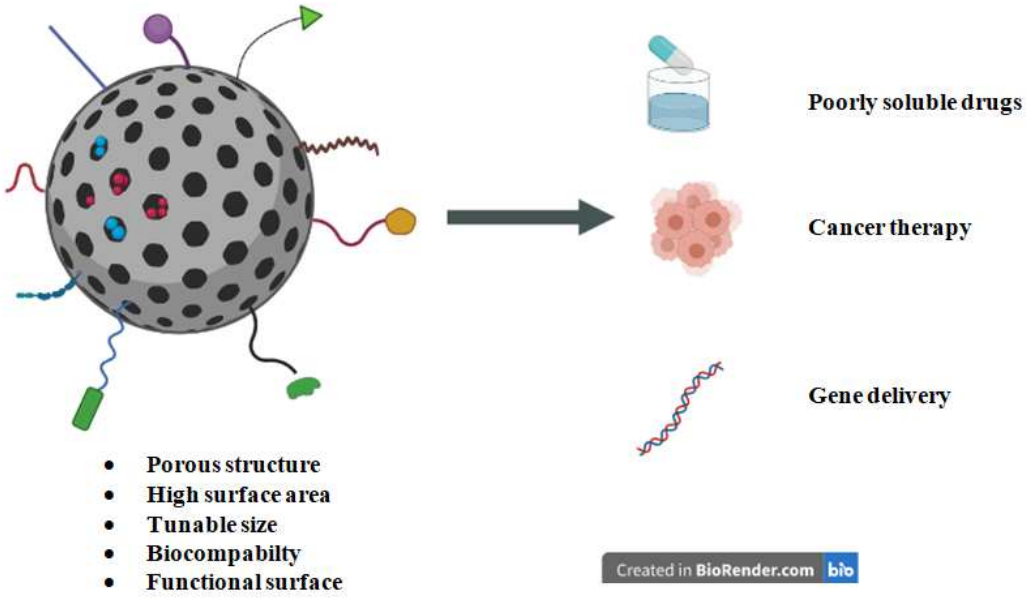

Figure 3. Mesoporous silica used in cancer therapy applications, gene delivery, and to deliver poorly soluble drugs due to its high surface area and suitable pore-volume ratio (Created with BioRender.com).

2.5 Core-shell particles

The particles used for drug delivery were core-shell systems, also known as core-shell composites. These systems are made of a core and a shell, each built from different materials with varying functions, depending on the loaded drug (Galogahi et al., 2020).

The reason core-shell composites are widely used in drug delivery systems is due to their potential in different fields such as bioimaging, controlled drug release, tissue engineering, and different disease treatments. This versatility among different fields made core-shell particles a highly-researched topic over past decades (He et al., 2015).

A common material used for composition shell is MSN. This is due to their high surface area, controllable diameter of pores, uniform mesoporosity, biocompatibility, surface friction, ability to control core size, and its thickness. These features allow researchers to build desired composites and fill them with a desired drug. For the drug-loaded particle to be released in the system, there must be stimuli which will activate the drug release. MSN has many different possibilities to open nanopores, such as temperature, PH, enzymes, light, redox activation and competitive binding, in order to let the drug molecules in the targeted cells (He et al., 2015)**.**

The synthesis of the core-shell system is usually done through a multiple-step process, where the core is synthesized first, followed by the shell. The process depends on the morphology and materials used. The goal of these core-shell systems is to produce a stable particle with biocompatible properties (Hayes et al., 2014).

A good core composite of core-shell system is cerium oxide nanoparticle (CeO_2) surrounded by MSN, as was used in this project as the drug delivery system. The synthesis is a two-step process, as described above. The CeO_2 is widely used as a therapeutic agent in reducing the inflammation and in treatment for oxidative stress-associated chronic diseases. It is nontoxic to living cells, with the capability to disable many reactive oxygen species (ROS) correlated with causing different diseases (Cooper et al., 2014)**.**

2.6 Drug delivery

Drug delivery is the process of transporting and releasing a drug to a targeted tissue or organ by nanoparticles. The drug release is performed under controllable conditions, meaning that the drug needs to be released at a certain point in time under specific conditions (Peppas and Narasimhan, 2014). If the drug release is premature or delayed, it can cause problems in disease treatment. Every drug delivery particle needs to have a controllable point, where it does not release the drug in order to protect healthy cells, in order to target only diseased cells. If the drug release would be rapid and constant in the body, this would lead to dangerous consequences (Cooper et al., 2014).

When the drug-loaded particles are in the body, messengers are helping to deliver them to the targeted cells. In order to reach targeted cells, chemical and physical properties of the drug delivery systems need to be satisfied. As described already, nanoparticles provide many adjustable parameters, and the structure can be designed for optimal drug encapsulation, such as, the size and polymer coating for the nanoparticle. The nanoparticles in the project were built under specific procedures, as they had to be uniform and of a certain size (He et al., 2015).

Particle size is one of the most important factors in a drug delivery system. The nanoparticle size can affect the distribution of the drug within nanoparticles, affecting the efficiency of the drug (De Jong and Borm, 2008). Antibodies bind to any foreign molecule and build the immune system. Using smaller nanoparticles decreases the chances of them to bind to antibodies in the blood, meaning smaller nanoparticles have a higher chance to deliver the drug to the wanted area without unnecessary interference. Tissue uptake of the nanoparticles is higher as the size of nanoparticles is smaller (Han, 2016). Another important factor affecting the biological properties of the nanoparticles is their shape. The uniform shape of nanoparticles increases the binding probability, drug delivery, and cell uptake due to greater prevalence in the blood stream and the body. Therefore, using smaller nanoparticles with a uniform the shape lead to more successful results (Cooper et al., 2014).

2.75-aminosalicylic acid

The drug tested in this experiment is 5-ASA, and it is thought to be anti-inflammatory because it reduces inflammation in the damaged tissue at the metabolic level (Xu et al., 2004). It is attracted to ROS, which are present in inflamed joint, therefore it is expected to target the OA site and reduce inflammation.

5-ASA has low solubility in the water and, when inserted in the blood circulation, will not dissolve until it reaches the targeted cells. In the occurrence of OA, the number of ROS is increased in the inflamed joint area. Knowing this, it is possible to conclude that 5-ASA, anti-inflammatory drug, would target the affected joint area, due to increased number of ROS (Askelof and Helander, 1992).

In recent years, there have been new 5-ASA drug discoveries, with improved pharmacodynamic and pharmacokinetic properties for the treatment of different diseases. Chemical and physical properties of the 5-ASA structure include low solubility in water,

and the physical structure is determined by the temperature, meaning that the drug would not dissolve in the blood, and would not be spread all over the healthy cells, just the targeted area, under certain temperature (Abdu Allah and A El Shorbagi, 2016).

If the 5-ASA drug is inserted in the body by itself, it creates instable environment by having low solubility in unwanted area affecting the healthy cells as well (El-Dairi and House, 2019). Due to these circumstances, scientists are focused on minimizing the solubility rate of the 5-ASA drug and extending the absorption time causing no harm to the body, maintaining the high drug concentration. The tested drug satisfies mentioned conditions, if it is a part of the microparticle carrier system. When it is encapsulated within molecule, 5-ASA stays longer in the blood, does not damage healthy cells, and creates stable environment.

Due to the lack of the solubility of 5-ASA, patients need to take high doses to fulfill the effect of the drug. Due to those high doses, patients face many reactions and side effects, such as vomiting, fever, headache and even eating disorders. To resolve complications, biocompatible drug carriers are used for targeted drug delivery to control the release and minimize side effects (Abdu Allah and A El Shorbagi, 2016).

In the project, 5-ASA was added to the micro compositions made of CeO_2 core and MSN shell, coated with a PEO-b-PFMA. By using nanoparticles loaded with the drug, it was expected that the drug would go to the targeted area and release 5-ASA drug without any harm to the healthy tissue, with minimal side effects (Abdu Allah and A El Shorbagi, 2016).

2.8 Gold nanorods

Gold nanorods are new, promising gold nanoparticles for drug delivery systems. Due to their strong absorption in near-infrared (NIR) light region, gold nanorods have strong photothermal effects, as well properties such as reduced photobleaching effect, making them widely used for bioimaging applications. The reactivity of particles could be improved by controlling the optical properties, size, and shape of gold nanorods. With these properties, it is of great interest to construct a drug release system where the release can be controlled with this metal (Huang et al., 2009).

Gold nanorods play an important role in drug delivery and in targeting desired tissue area due to their nano-scale. Gold nanorods can be absorbed by visible NIR depending on their shape and size, and have high surface area, making them ideal nanocarriers (Arvizo et

al., 2010). The desired size enables targeting wanted region of interest, as well as possibility of longer lifetime for imaging. Due to those properties, they are used in photothermal responsive therapy, and as a bioimaging agent. It is possible to locate nanorods in the complex areas in the body, such tissue parts containing different cell types, so they are an ideal candidate for the targeted drug delivery (Huang et al., 2009).

The gold nanorods constructed in this project were polymer-coated. The function of polymer was to act as a drug reservoir, where the drug was not prematurely released, or it was released at the minimum level. Another reason of polymer coating was to smoothen the surface of the particle so it would not damage tissues (Haine and Niidome, 2017).

2.9 Polymer coating of the particles

The rapid development of nanotechnology and its use in drug delivery is widely applicable and can be adjusted as needed to fit different project aims. The high surface area, surface energy, and the small size of the particles, lead to a need of adaption with the specific chemical and physical properties. The properties such as the lubricated surface, biocompatibility, and ability to bind to targeted molecules, in order to fit the project goals. Coating nanoparticles for drug- delivery systems with the thin, but functional polymer needs to be performed to control the drug release (Liechty et al., 2010). Polymer thickness can affect the drug release by preventing the drug to exit the microparticle system if it is too thick. A suitable polymer is needed to fit experimental needs, such as control of how much and when a drug will be released. Polymer coating of nano- and micro- particles can be challenging due to the size of particles (Wang et al., 2004)**.**

The polymer of interest in coating of particles in the project was poly (ethylene oxide)-b-poly (furfuryl methacrylate) (PEO-b-PFMA). This exact polymer has an advantage of controlled drug release, not affecting the tissue. The lubricated smooth surface does not damage the living cells. Controllable physical and chemical properties of PEO-b-PFMA allow researchers to get the wanted results in the relatively short time period. Using microfluidics in droplet production of polymer, allow the control of the polymer synthesis under live time microscopy.

The main benefit of PEO-b-PFMA as a part of drug delivery system is that effect on a healthy tissue is minimal. Because of NIR light, the control of the light-responsive

drug release is possible. That way the amount of the drug released is controlled, and there is no excessive amount of drug released which can damage the tissue. NIR is less damaging for the tissue, so frequently used for in vivo therapy. Usually gold nanorods are encapsulated with PEO-b-PFMA polymer, which represents photothermal agents and trigger the drug release (Salma et al., 2018).

The challenge to coat particles is their small nano- and micro- size. By using microfluidics, opens different possibilities (Mazetyte-Stasinskiene and Köhler, 2020). The needed modification of the particle surface, by polymer coating, allows researchers to try different methods. Finding suitable method can be a time consuming, but once the perfect method is decided, the process of encapsulation is fast. This new way of controlling physical and chemical properties of the surface for the targeted drug delivery system, is getting more accepting in the future research in drug delivery.

2.10 Microfluidic Device

The combination of different fields such as chemistry, biochemistry, biology, physics, nanotechnology and biotechnology represents one of the most common areas associated with the drug delivery and pharmacokinetics which is called microfluidics. It is closely related to optofluidics because of constant uses of optics and imaging devices to manipulate fluids on nano- and micro- scale (Zhao et al., 2020).

Microfluidics allows possibility of developing complicated experiments under live microscopy on a chip. The benefit of using microfluidics is that the smaller amount of chemicals is needed to perform the experiment, which makes them more affordable. By using smaller amount of chemicals, the experiment process is shorter, which is one of the most important criterion in drug delivery.

The microfluidic device enables the precise handling of a liquid with the help of miniaturized capillary networks. The platform contains PHD ULTRATM Syringe pumps shown in figure 4. The platform controls the number of chemicals used by push-pull controls. One pump contains two racks, one for the inner and one for the outer fluid inserted in the syringes. Under the high pressure, desired nanoparticles can be loaded with a drug.

Finding different pump speeds for the inner and outer syringe is the only tricky part of using the microfluidic pumps. Usually, the outer syringe uses a higher speed, around 30-40

mL/hour. The inner syringe containing nanoparticles uses a slower releasing speed, around 2-5 mL/hour. Deciding what speed to use is important, because it defines droplet size and how nanoparticles will be loaded with the drug. It is important to try different pump speeds and then image the final drug-loaded nanoparticles using TEM. If the product size and appearance are satisfactory, it means the pump speed was set correctly (Beebe et al., 2002).

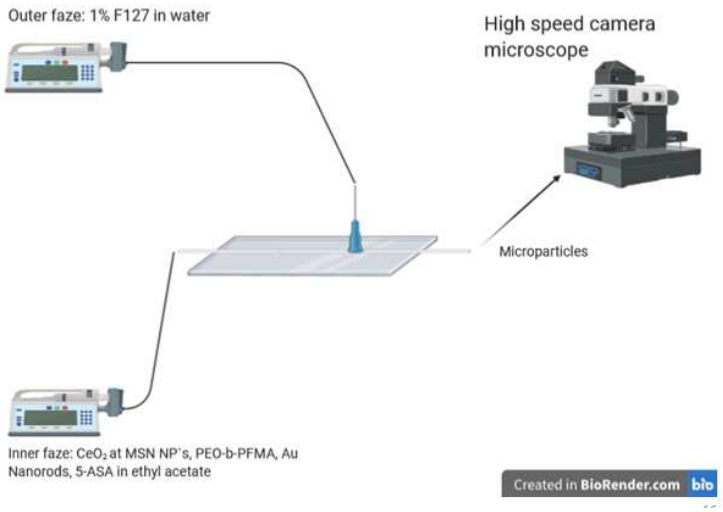

Figure 4. Representation of the microfluidic device, containing two pumps for pumping fluids inside the chip, and a high-speed camera microscope for observing droplet progress. (Created with BioRender.com)

The experiment is taking place inside the chip. The design of the chip can be constructed in the laboratory by the researcher depending on the wanted final results. Every experiment requires a specific kind of a chip. There is another possibility to purchase different kinds of chips from some companies, but it is costly. All chips have an expiration date, after certain amount of experiments preformed, they get damaged. It is necessary to replace them so the final results are not affected.

Before constructing the chip, it is important to consider some effects to obtain the wanted results, and to predict how the chip workflow should behave, therefore the understanding of physics is required. The important effects that should be taken under consideration are surface to volume ratio, tension, fluidic resistance, diffusion, and the most important, laminar flow (Beebe et al., 2002).

Using microfluidic pumps to push fluids inside the chip applying force direct fluids flow to be almost always laminar. Laminar flow represented in the figure 5a, shows the state in which fluids flow is not considered random, flows in parallel layers with no

disruption between them. To mix two or more fluids, diffusion is necessary. Laminar flow gives the possibility to create flows that maintain the wanted formation allowing the production of droplets inside solution. By using microfluidics, it is possible to control the speed of the fluids, the size of the droplets and their properties (Jokinen, 2017).

5a

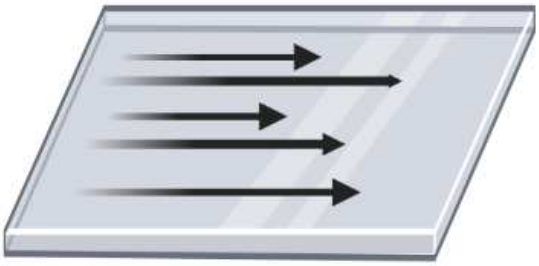

5b

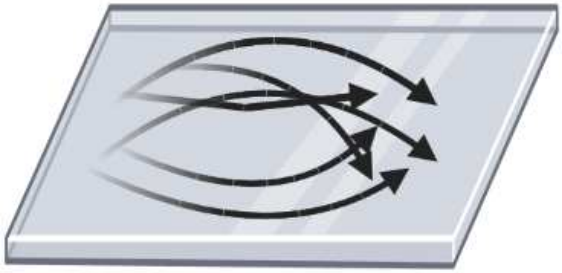

Figure 5a Laminar flow in a capillary, which is one of the most important effects in the microfluidic system. (Created with BioRender.com)

Figure 5b Turbulent flow with high momentum convection (Created with BioRender.com)

To control if the droplets are similar size, as well as what amount of inner and outer fluid to use during the syringe injection and mixing, a high-speed digital microscope is used. Image 1 was taken with the Meros High-Speed Digital Microscope, designed for microfluidics and used for observing droplets during high-speed droplet production (Snp and Reagent). High-resolution imaging is possible with the advantage of the short exposure time. It is possible to connect the microscope to the computer screen to make images or videos of the droplet formation. The use of the microfluidic platform enables control of the droplet size, even distribution, and the speed of mixing inner and outer fluid.

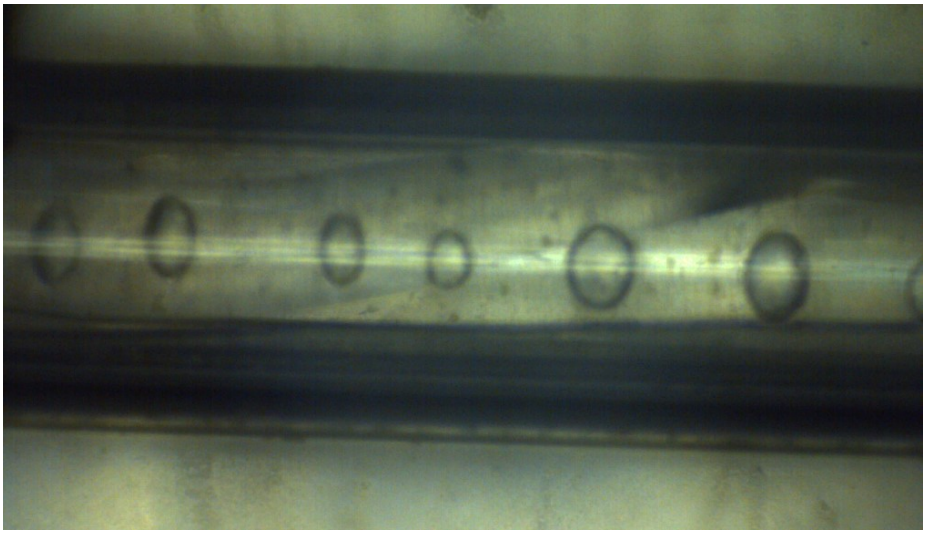

Image 1. Droplet formation inside microchip visible from the live time microscope.

Taking into consideration all physics concepts previously mentioned, it is possible to construct the laboratory on the chip and manipulate fluid flows on microscale levels. Microfluidic systems bring significant meaning for the use of bioparticles in clinical diagnostics where time is essential (Zhao et al., 2020).

The Microfluidic system is closely related to optical imaging. The importance of live microscopy is significant and gives the possibility to track the droplet making progress, as well as constant monitoring during experiments. The combination of live optic images and microfluidic machine gives a low-cost solution (Zhang et al., 2011).

3 HYPOTHESIS AND AIMS

The process of drug delivery gained a lot of interest in the last decade, as new research opened the door for new possibilities and information on this topic. Drug delivery is the procedure of transporting and releasing a drug to a targeted area. This can be done using nanoparticles, which have also gained interest in the scientific research field, as nanoparticles have controllable properties and allow for easy modification. Drug delivery systems made of nanoparticles, allow researchers to perform drug release under specific conditions. Drug systems can be modified to target a desired area, without damaging surrounding healthy cells.

While drug systems composed of nanoparticles offer many benefits, there are limitations to synthesize them. Limitations could be that syntheses are time consuming and produced particles may fuse, which is leading to a need for optimizing the synthesis process. Another limitation includes optimizing the amount of the drug used. It is necessary to find the right drug-to-nanoparticle ratio. If there is too much or too little drug in the nanoparticle, the drug will not be beneficial for the treatment. A suitable and functional polymer that does not interfere with nanoparticles must be found, to protect surrounding healthy cells when delivering the drug to the targeted area. These often time-consuming challenges must be addressed and optimized in order to develop a functional drug delivery system.

One way to begin optimizing the synthesis of drug delivery systems includes using microfluidic systems as a drug loading systems. Using such system allows for easy manipulation of fluids used during the synthesis on nano- and micro- scale. Building drug delivery systems using a microfluidics system is done by using a small chip, where two fluids are pumped inside with different pump speeds, producing droplets. By using microfluidic system, smaller amounts of chemicals are needed, making experiments more affordable. Using live microscopy makes it possible to control the droplet production in the chip. Microfluidics allows for a bulk production of nano- and micro- particles, making the process time efficient.

The same microfluidics method is also used to load desired drug into the CeO_2 within MSN nanoparticles. By manipulating the pump speeds for the different fluids, it is possible to load the drug to make the functional drug carriers.

The final step producing a drug delivery system is to coat the synthesized nanoparticles with the suitable polymer. Loaded nanoparticles can be added to desired polymer pallet with the pipette.

The aim of the study was to optimize drug delivery systems to deliver the drug to treat OA by controlling chemical and physical properties of microparticles. By optimizing different amounts of the inserted drug, the thickness of the polymer and the size of the CeO_2 within MSN nanoparticles, it was hypothesized that this would make an ideal nanoparticle drug delivery system. In the future research, built microparticles can be tested in vivo to monitor how the drug works, and how fast delivering the drug to sites of OA will lead to decrease the inflammation.

4 MATERIALS AND METHODS

4.1 Construction of the microfluidic chip

Drug development with the microfluidic technology has rapidly expanded in recent years. The microfluidic chips provide a new understanding of drug research, making experiments more affordable and less time consuming. The possibility of constructing the chip for usage in the droplet production, gives the chance to control all the factors needed for the successful experiment (Cui and Wang, 2019).

To conduct drug encapsulation within nano- and micro- particles, the application of microfluidic chips is necessary. The microfluidic chip is built using set guidelines, depending on the function of the drug delivery system. The chips used for the study contain glass borosilicate capillaries, through which fluids flow. The inner thinner capillary, with the diameter of 1.1 mm, is inserted in the thicker capillary, with the diameter 1.56 mm. The difference between diameters provides wanted capacity for the mixture of fluids. The difference between capillary sizes is also important for controlling the fluid droplet size and flow inside the chip.

The chip production was performed in the laboratory inside hood to prevent external agents from interfere with work, as shown in image 2. The equipment for constructing the chip included glass capillaries, black sandpaper, diamond cutter, Devcon 5 Minute Epoxy glue hardener, a PN-30 Magnetic Glass Microelectrode Horizontal Needle Puller, syringe cups, tweezers, and a gas torch flame gun.

Image 2. The chip production area inside the hood with all necessary equipment to prevent external agents from interfering with work.

The inner capillary was separated with a PN-30 Magnetic Glass Microelectrode Horizontal Needle Puller (Narishige, Tokyo, Japan). This device is capable of separating glass capillaries in two parts using a heat source and a magnetic puller, separating the inner capillary into two smaller conoidal parts. The separation was possible due to the heater which uses platinum plate to heat the glass. The magnetic puller, using the electromagnetic force, pulled the glass capillary in the opposite direction. The glass capillary was separated at the exact point where the heating was performed (One Digital Drive, 2018). One of the capillary parts was then used to shape the droplet size. To do this, the capillary was gently scraped with the black sandpaper at the conoidal end to create an opening. The scraping was monitored using a light microscope. This opening formed the droplets within the chip.

The thicker outer capillary is longer than the inner capillary. Metal tubes are inserted and glued in the outer capillary at the glass surface using the Devcon 5 Minute Epoxy glue hardener to hold the tubes in on the glass surface and prevent the leakage of the fluids. For the glue to harden, 24 hour drying was necessary. The outer capillary was then cut and glued at certain places to prevent mixing of the fluids. Figure 6 shows these cut openings at two places. The first opening was cut at the outer glass capillary, right after the metal tube. The function of this opening was to prevent the backflow of the fluids after mixing inside the chip. The second opening was cut within the syringe tip in the middle of the chip. Its function was to open up the passage for the outer fluid to be delivered within the chip. Both openings were glued to prevent the fluid spillage and to keep the capillaries on the glass surface.

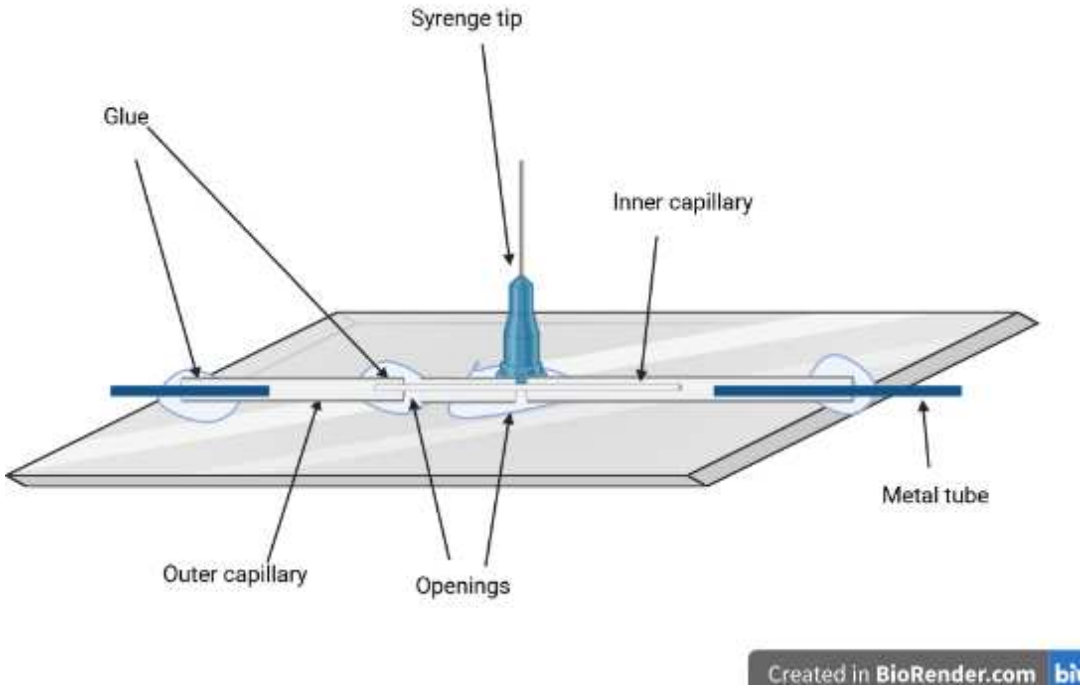

Figure 6. Replica of the chip used in the project (Created with BioRender.com). The chip contains two openings, two metal tubes, inner and outer capillaries, and the syringe tip. Openings are pointed with arrows and glued to the glass surface. First opening is placed right after metal tube in order to prevent leakage of fluids within the chip. The second opening is placed under the syringe tip and acts as the passage for the outer fluid to enter the chip.

4.2 Synthesis of cerium oxide nanoparticles

We used CeO_2 NPs in the experiment as the drug carrier for targeted drug delivery. CeO_2 NPs were produced as the core of the nanoparticle, with Mesoporous silica nanoparticles (MSN NPs) as the shell. The drug was loaded between the CeO_2 core and MSN NP shell.

The mixture process of CeO_2 NPs was divided into two steps: Precipitation and Aging. To perform the following protocol, the method by Jixiang Wang 2019 (Jixiang Wang, 2019) was used.

For the precipitation process, 4.3 g of $Ce(NO_3)_3$ crystals (MERC, Darmstadt, Germany) were dissolved in 50 mL of MiliQ water, which was previously dissolved in a 100 mL round bottom flask. The solution was placed in an oil tub, warmed to 70 °C and stirred at 500 RPM. During stirring, 3M ammonium hydroxide at a pH of 7.5 was prepared

by mixing 14.569 mL of ammonia solution with 10.405 mL of MiliQ water. To fix the pH of the prepared solution to 8.6, the following procedure was performed. Ammonium hydroxide 6 M solution was prepared by adding 1.239 mL of ammonia solution to 1.761 mL of MiliQ water, and the final product PH was 8.8. The final product was incubated for 20 hours at room temperature, and a white precipitate was formed. Next, it was necessary to perform three centrifuges, 10 minutes each at 8,000 RPM and 21°C. The solution was placed in the 50 mL Falcon tubes. After the first centrifuge, water was thrown away, and replaced with 99% ethanol for the next two centrifuges. After the final centrifuge, the product was dispersed in the MiliQ water, and stored in a 50 mL plastic tube.

4.3 Synthesis of cerium oxide within MSN

The MSN shell was synthesized following the production of the CeO_2 core. In a 100 mL round bottom flask, 125 µL of CeO_2 core was added, followed by 2.5 mL of MiliQ water. The mixture was held in a sonification bath for a couple of seconds, then vortexed. Mix 1 was prepared by adding 4.3 mL of MiliQ water with 2.9 mL of absolute ethanol, and 40 µL of ammonia. The previously prepared CeO_2 core solution was mixed with the mix 1 to form mix 2. The solution was placed in the sonification bath for 30 minutes and was vortexed occasionally. Mix 3 was prepared by adding 40 mg of CTAB in 660 µL of MiliQ water and 300 µL of absolute ethanol. Mix 3 was combined with mix 2 The final mixture was placed in the sonification bath for another 30 minutes. During the five minutes of sonification, 80 µL of TEOS was added. The mixture was stirred overnight at the speed of 450 RPM, and then stored in a plastic tube.

4.4 Extraction of synthesized Cerium Oxide within MSN

To extract the CeO_2 NPs, the previously prepared solution described above was placed in centrifuge tubes. The tubes were centrifuged three times for 10 minutes, at a speed of 12,000 RPM and 22 °C temperature. Before each centrifuge, the product was dispersed in the absolute ethanol (Etax, 99%), and placed in a sonification bath for six minutes, and vortex for four minutes. After the final centrifuge, the product was dispersed in 10 mL of absolute ethanol, and then analyzed under TEM. The size and appearance were recorded (Jixiang Wang, 2019).

4.5 Synthesis of PEO-b-PFMA

To lubricate the surface of the drug delivery system, *poly* (*ethylene oxide)-b-poly* (*furfuryl methacrylate*) (PEO-b-PFMA) was used. Preparation of the macroinitiator began with the mixing a 0.915 g (7.5 mmol) sample of Dimethylaminopyridine (DMAP) in a previously mixed 0.505 g (5.0 mmol) of Triethanolamine (TEA) and 20 mL of dry methylene dichloride (CH_2Cl_2) in a 100 mL flask. The mixed solution was move into a 250 mL three-neck round-bottom flask. The middle neck of the flask was connected to condenser, the right neck to a gas inlet/outlet, and the left neck was used for a dropping funnel opening. After placing a magnetic stirrer in the flask, the temperature was set to 0°C. After cooling the solution, 2.875 g (12.5 mmol) of α-bromoisobutyryl bromide previously mixed in 20 mL of CH_2Cl_2 was added. Then next step was to form a yellow dispersion by adding 25 g (5 mmol) of Poly (ethylene oxide) (PEO) in 100 mL of dry CH_2Cl_2 dropwise during the time period of 1 hour. Dry nitrogen gas was connected to the right inlet/outlet gas neck of the flask, and light stirring was performed. Afterwards, the temperature was slowly raised to 21°C. The stirring was continued for 18 hours, then, the solution was filtered using filter paper. During filtration, half of the solvent evaporated, while other half of the product was mixed in cold diethyl ether. Suspension of the product in absolute ethanol was then performed. The solution was stored at the room temperature for at least 12 hours in order to recrystallize the product, as shown in image 3. The final product was filtered using the filter paper, and then washed again in cold diethyl ether. The final product was then dried in a vacuum overnight (Sun et al., 2005).

Image 3. The white subtract which was collected after the microfluidic process of preparing PEO-b-PFMA macroinitiator.

4.6 Optimization for PEO-b-PFMA microparticle formation

The previously- prepared PEO-b-PFMA macroinitiator was mixed with the 8% Ethyal acetate in order to be used as the inner fluid for the microfluidics. To dilute the percentage of the 99.5% Ethyal acetate, it was necessary to mix 8 mL of the solution with the 92 mL of MiliQ water.

The next step was to optimize how much PEO-b-PFMA is needed for the formation of the particles after microfluidics. This part of the project was challenging due to many tests of different concentrations to form droplets, then microparticles. This was the first step of three for creating the final inner fluid to form drug delivery microparticles. The difficulty in optimization includes the many different possible combinations which should be tested to choose the most suitable one. The loading process is the same with all different concentration tries, with the fluid being inserted into the syringe and attached to the PHD Ultra Advanced Programmable Syringe Pump. When the pump was activated, it pushed the fluid into the chip, where droplets containing polymer particles are formed. The pump was easily manipulated to adjust the desired speed. The final product was collected inside small glass flask. Image 4 shows the microfluidic device set up in the laboratory.

Image 4. The microfluidic platform for droplet production. The platform is made of two pumps, MEROS live microscope, and the computer screen.

The previously-prepared PEO-b-PFMA macroinitiator and 8% Ethyal acetate mix was inserted in the 5 mL Becton Dickinson Plastipak syringe for inner fluid. The outer fluid used was 1% Pluronic F127 diluted in the MiliQ water. To prepare the 1% solution, 1 g of Pluronic F127 was diluted in the 100 mL of MiliQ water. The second Becton Dickinson Plastipak 30 mL syringe was connected to the pump as well. It was possible to adjust the flow rate of each syringe. Finding the functional speed was the critical point in the polymer synthesis. Different settings allow setting the speed for the inner fluid in μL/hr, while the outer fluid setting could be μL/min. This volume per time scale setting allowed setting up different purpose speeds, which was significant, but time consuming in the optimization.

The goal for this part of the optimization was to figure out which fluid flow speed to use in order to form appropriately-sized droplets containing PEO-b-PFMA polymer. The recommended speed for the inner fluid was 2 mL/h, and for the outer fluid 40 mL/h. This speed was the starting point of the optimization. The droplet formation was observed using live microscopy, as described above.

When the droplets were formed and collected in the glass flask, this flask was carefully covered with the foil and placed under the hood to avoid the external influences as they were left overnight to become more stable. SEM was used to study the surface of the particles in order to determine whether the particles were not dissolved, and to decide if the microfluidic experiment was successful. TEM was also available for the imaging of the particles, where the size was measured, and different sections of the particles were scanned.

4.7 Optimization for coating CeO_2 within MSN with PEO-b-PFMA

When the desired particle size was obtained, the product was prepared for the coating of the previously prepared CeO_2 nanoparticles. The process was performed by adding the CeO_2 pellet with the pipette to the polymer. The process needed to be performed carefully, with gentle mixing, so the polymer particles would not end up fusing together.

This previously mentioned process presents the second step in the three-step procedure, following with the adding the 5-ASA drug. Before adding the drug, it is necessary to check with the SEM and TEM, in order to see if the polymer coating was successful.

4.8 Optimization for adding 5-ASA drug to the mixture

The last step in the development of the drug delivery system would have been adding 5-ASA drug to the mixture of CeO_2 and PEO-b-PFMA. The project was stopped as unforeseen circumstances did not allow enough time to optimize the polymer particle development.

4.9 The synthesis of the gold nanorods

Gold nanorods were built following the protocols from a guide (Scarabelli et al., 2015). The procedure used from the guide consisted of two parts: preparing the seed at CTAB for single-crystal Au preparation, and the growth of Au NRs.

First, however, CTAB (MERC, Darmstadt, Germany) was prepared as a stock solution. In a 100 mL round bottom flask, 50 mL of MiliQ water was added. The flask was put in the heated water bath and the temperature was set to 30 °C for CTAB to be dissolved. Following this, 1.82 g of 0.1 mol CTAB was added and steered. When the color of the solution turned completely clear, the solution was ready to be used and able to be stored for longer periods. Synthesis of a single crystal gold nanorod was performed in a steering water tub at a temperature between 27- 30 °C. A new 50 mL round bottom flask was put in the water tub with the temperature set on 30 °C. After placing the stirring magnet in the flask, 4.7 mL of the CTAB solution was added.

Next, solution prepared was a mixture of 16.98 mg of Chloroauric acid ($HAuCl_4$) (China, check) in one mL of MiliQ water. The mixture was added to CTAB solution. After the solution became yellow, 25 µL was added to the CTAB solution. The mixture was stirred slowly for 5 minutes. During the stirring time, 10 nmol Sodium Borohydride ($NaBH_4$) (MERC, Darmstadt, Germany) stock solution was freshly prepared by adding 7.6 mg to 20 mL of MiliQ water, where the 300 µL was rapidly injected in the previously prepared mix under vigorous steering with a speed of 1200 RPM. After 20 seconds, the steering speed was decreased to 400 RPM, and the solution was stirred until the solution became light brown. The product was stored in a temperature between 27 - 30 °C to prevent CTAB crystallization.

The next step, described as the growth process was to synthesize single-crystal Au NR's. First, a stock solution of 1 M Hydrochloric acid (HCl) was prepared by mixing 10 mL of 37% HCl (MERC, Darmstadt, Germany) with 110 mL of MiliQ water. A round bottom

flask of 50 mL was placed in the water tub with the temperature set on 30 °C, and 190 μL of HCl was added. After gentle stirring, 100 μL of $HAuCl_4$, prepared as described above, and 10 mL of CTAB were added to the flask. The solution was gently stirred for 5 minutes. During this time, 10 nmol Nitric Acid ($AgNO_3$) solution was prepared. $AgNO_3$ solution needed to be freshly prepared by adding 17 mg to 10 mL MiliQ water. Next, 120 μL of Nitric Acid was added to the solution and lightly stirred. The final stock solution prepared was 100 mM Ascorbic acid ($HC_6H_7O_6$), which was done by adding 176 mg of $HC_6H_7O_6$ to 10 mL MiliQ water. By adding 100 μL to the mixture, the cloudy solution became clear.

The final step in preparing Au NRs was to add 24 μL of seeds at the CTAB, prepared previously, strongly stir for a couple of seconds and then left to rest for two hours in the water tub at 30ºC. The final product became dark purple and was ready to be checked under TEM (Scarabelli et al., 2015).

4.10 Optimization for creating final microparticles

Final optimization was simplified in order to speed up the process. The original plan was to build microcomposites containing core-shell nanoparticles CeO_2 at MSN, 5-ASA drug, gold nanorods, all coated with the PEO-b-PFMA. The simplified version was decided to remove the gold nanorods, to reduce the time of the project.

In this new case, microfluidics would be necessary to build the final microcomposites. For the inner fluid, CeO_2 at MSN and 5-ASA with the PEO-b-PFMA would be all put together in Ethyal acetate. The inner fluid plastic syringe of 5 mL would be inserted in the pump system. The outer fluid would be 1% F127 mixed in the MiliQ. The outer fluid mixture supposed to make droplets stable enough to form microparticles. The outer fluid would be inserted into the 30 mL plastic syringe, and connected to the pump system. The fluids would be connected to the microfluidic chip used in the formation of the particles in the previous experiments. The speed of the inner fluid would be between 2 to 5 mL/h, while the outer fluid pump speed would be around 40 mL/h. The droplet production would be monitored with the live time light microscope, where images would be taken. The final product would be examined with TEM, and microparticles would be analyzed.

4.11 Microscopy

To obtain wanted results, and to check if prepared particles are wanted size, shape, and composition, imaging using Transmission electron microscope (TEM) and Scanning electron Microscope (SEM) is necessary. Microscope usage was present in every part of the project. Simple light microscope was used during the chip production, and Live Time microscope was used during droplets production.

To check the size and composition of the particles TEM was used, as shown in the image 5. This microscope works based on an electron beam, which is fired through a sample. Due to contact between electrons and atoms, it is possible to get a clear image of the structure. Electron microscopy samples were imaged in the Electron Microscopy Laboratory. The microscope located there was JEM-1400 Plus. It is a high contrast microscope with high resolution imaging capable of detecting nano-size particles. This microscope was specifically used for imaging CeO_2 nanoparticles, due to their nano- size. The microscope contains high- resolution sCMOS camera ("Matataki Flash") which captures images with low noise, which helps in image analyzes afterwards (Goodhew, 2011).

To monitor the production of the droplets, Meros High-Speed Digital Microscope designed for microfluidics, was used. It is a simple light microscope connected to the computer screen, imaging the live time. With this microscope, it was possible to monitor the crucial part of the experiment, which was droplet formation. A simple light microscope was used in chip production. It was possible to see if the glass capillary separation was successful, following the gap shape and size after using black sand paper.

After synthesis of the polymer, High-Resolution FE-SEM was used (Image 6). The model was Apreo FE-SEM + ED, Field-Emission Scanning Electron Microscope (FE-SEM) with EDS, CL and STEM capabilities. The main purpose of using the microscope was to observe if the surface of the polymer was synthesized correct. Main parts of the SEM are the electron gun, condensed lens, objective lens and scanning coil. An electron probe is produced by the objective lens in order to adjust its diameter. Electron beam is produced in the electron gun. A scanning coil scans the electron probe. Specimen and entire optical system is kept at vacuum (Weiss, 1983).

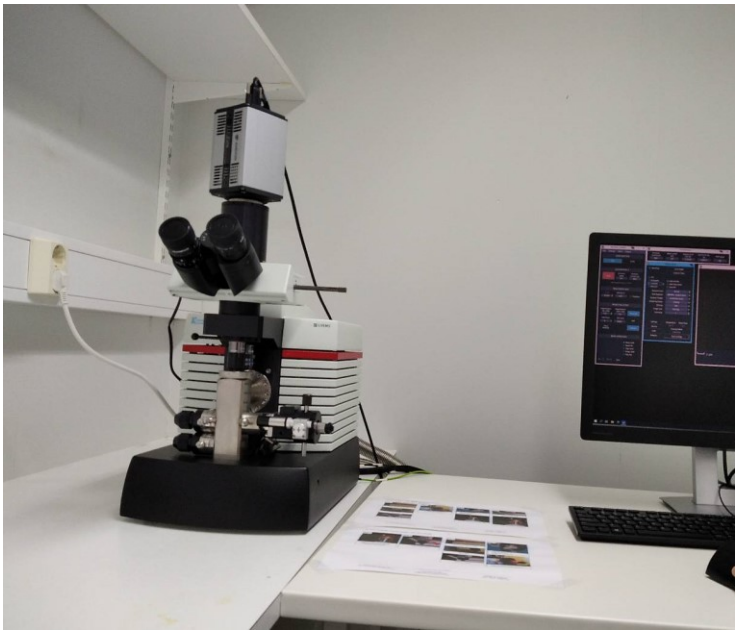

Image 5. The TEM microscope used for the imaging of final particles. The microscope is located in the Biocity on the 3rd floor.

Image 6. The SEM microscope located in the Faculty of Science and Engineering building.

4.12 Image analyses

The final and the most important step of the research is image analyzes. For the scientific analyzes, Fiji program was used. An image processing package is extended program offered by the ImageJ. The program offers different options to work with TEM and SEM images, to calculate and give the data needed in order to present results.

To analyze the image, it is important to prepare it in such a way that the end results are trustworthy. It is necessary to try different methods and use different functions in the ImageJ to set the most useful protocol in image analyzes. If the area of interest in the image is not visible to be analyzed, the part of interest can be isolated without destroying the result. One of the settings used was thresholding. It allows changing image pixels, in the other words, converts images from color to black and white. This simplified analysis helps to focus on a wanted part of the image, removing the part we are not interested in using as result. The program contains the option of adjusting the threshold automatically, which simplifies the process (Ferreira & Rasband, 2012)**.**

After adjusting the threshold, another possible function for the final analyze of the image could be creating masks. This function is used when the area of the interest of the image is over or under saturated, meaning that the image is converted to black and white based on the previous automatic threshold, where white and black in the histogram is presented by numbers, white as 0 and black as 255. If the image is oversaturated, function erode may be used, but in order to extend the wanted pixel, option dilate could be used. Another common and useful function is the ImageJ program is Watershed, which splits overlapping objects in the image. This option is useful if two nanoparticles in the TEM image are overlapping, and we want to analyze only single one.

To perform numerical analyses of the data, particle analyzes extracts wanted objects from selected section and analyzes them individually. It is possible to measure entire area of the interest. In that case, it is important that the image is converted to 8-bit, with the maximum values of 255, and minimum of 0. The useful filter which was used in the image analyzes was Gaussian blur, which removed the unwanted noise of the image (Ferreira and Rasband, 2012).

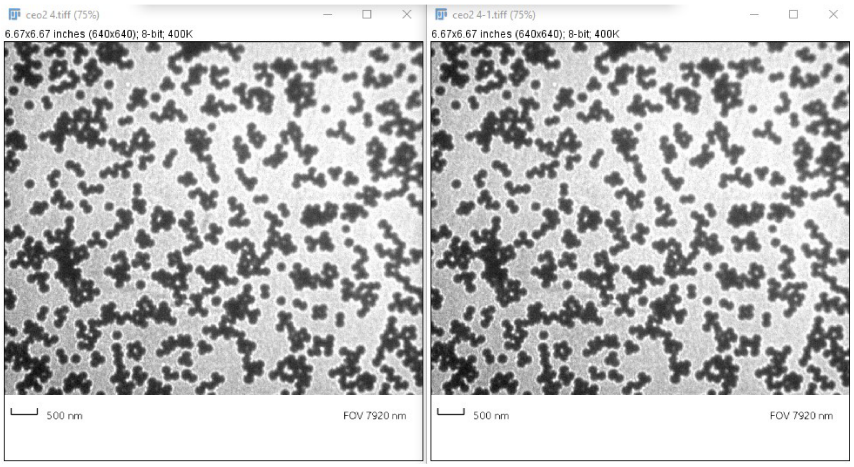

Image 7a. 16-Bit pixels are changed to 8-Bit (from color to grayscale), then duplicated in ImageJ program. The left side of the image is original starting image, while the right side image is the converted one.

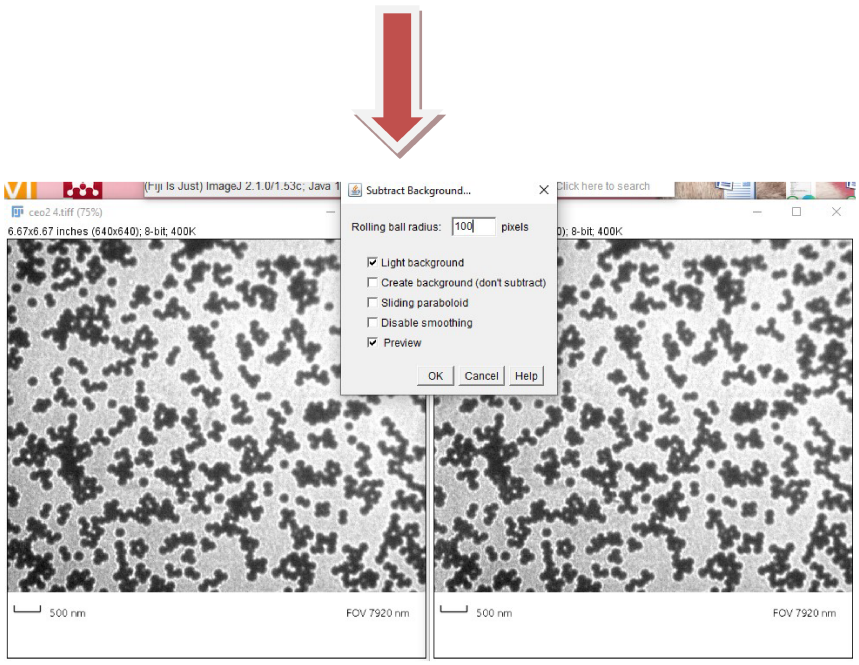

Image 7b. The background is subtracted from the duplicated image, with the rolling ball radius of 100 pixels.

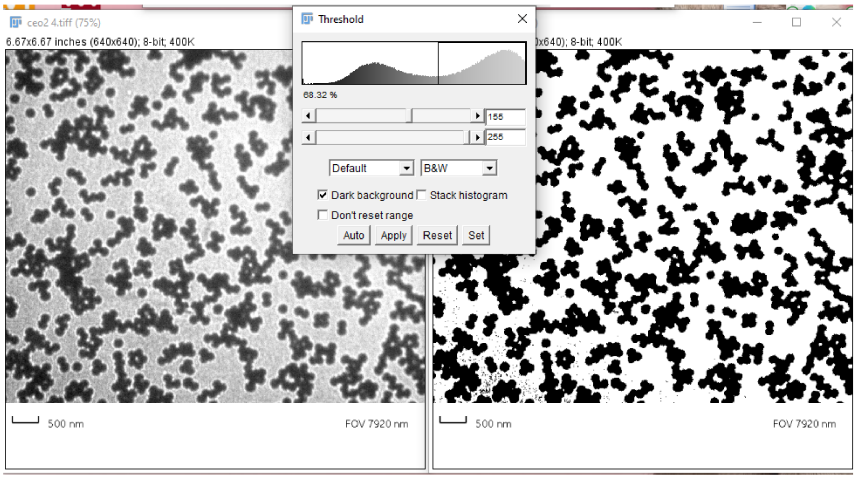

Image 7c. Manual threshold of 68.32% is selected with the dark background visible on the right side image.

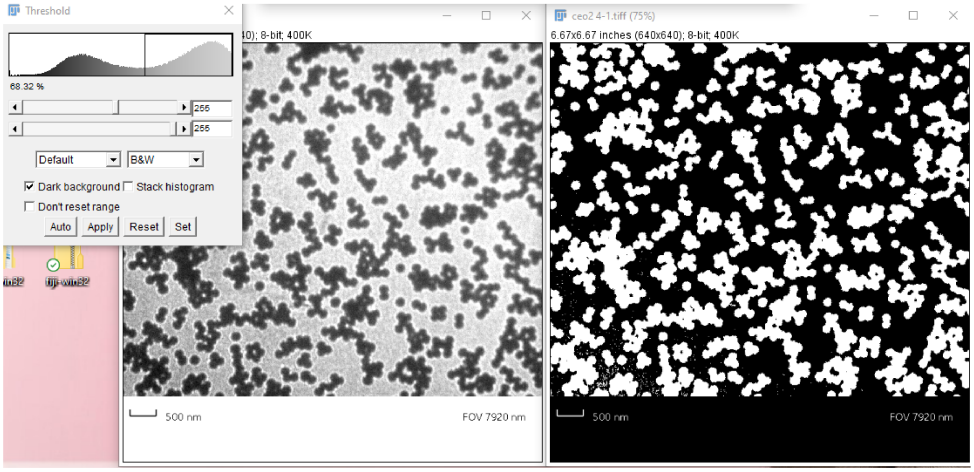

Image 7d. The image is converted to mask shown of the right side image.

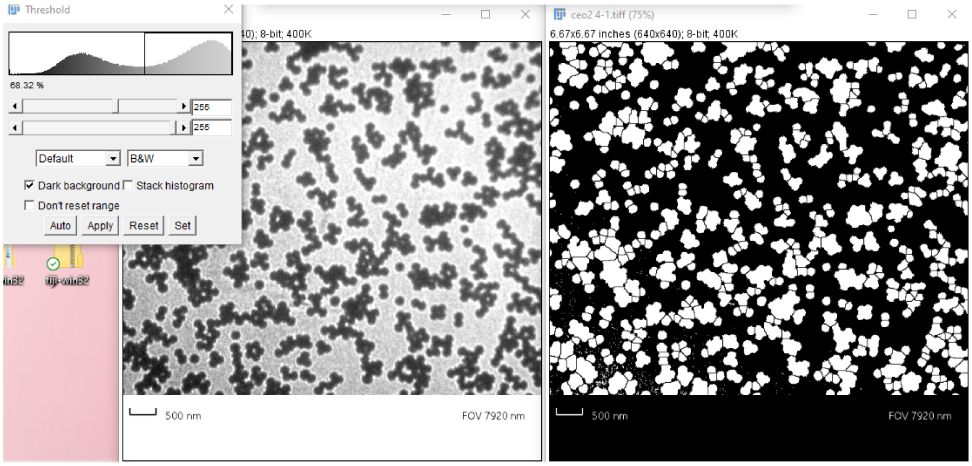

Image 7e. Watershed is the next step. Image on the right is presented with that filter.

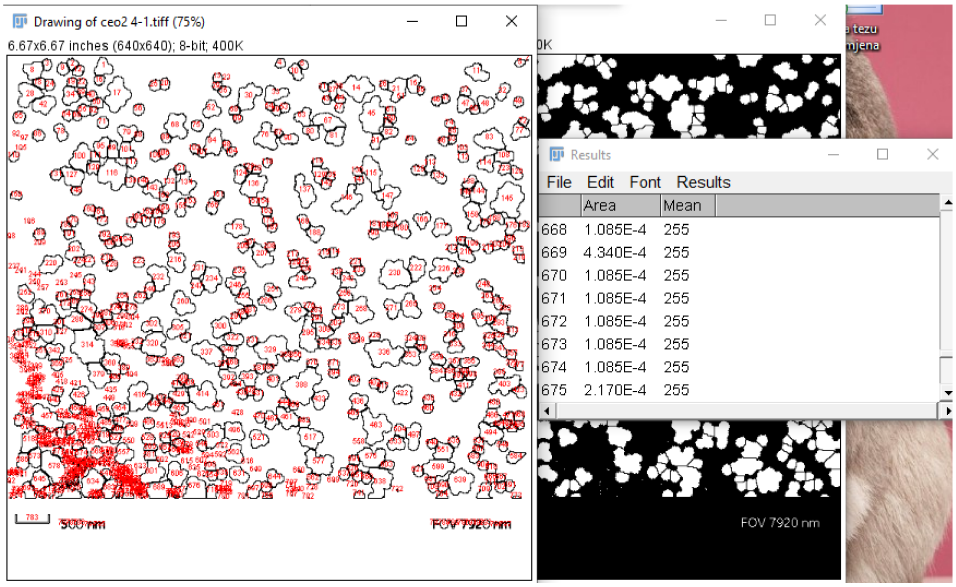

Image 7f. The final particle outline analyses results. The particle count is given, as well as area. Particles are surrounded with the black outline, each containing the red number inside the outline. In the table the number of the particle corresponds to its area.

Image analyzes was done in the following order: 1. Loading the image in the ImageJ, 2. Convert the image to the 8-bit, 3. Duplicate the image, 4. Subtract the background (ball radius around 100 pixels), 5. Manual Threshold (around 68.32% with the

dark background), 6. Select Convert to Mask, 7. Select the Watershed, 8. Analyze particles by the outline in pixels. The process is shown from images 7a to 7f.

In the final analyzes of the particles, the measurement was given in pixels (px). One px corresponds to 264583.3 nm (calculated by 2021 JustinTOOLs.COM). The scale bar presented in the image was given in nm and by simple calculation it was possible to convert the area from px to nm. Another option was to set the scale bar on each image to wanted size, in this case to nm. Then results of area were given in nm^2 or results of length were given in nm. This image analysis protocol could be used with the multiple SEM and TEM images. There are some adjustments needed in different steps depending on the image, and wanted end results.

This particular protocol was useful in analyzing TEM images where the area of interest was bigger and particles were overlapping. In the case of smaller area of interest, where the focus was on single particle, or just few of them, there was no need of certain steps. For an example, the watershed is not necessary, because the particles were not overlapping; the interest was just in the size and the structure of the particle. The useful step to add in that case would be Gaussian filter, to enhance the boundary of particles of interest. Gaussian filter focuses on edge pixels and corner pixels, rather than pixels inside the image, removing noise while keeping the edges of an object relatively sharp.

When analyzing particles, objects are measured and counted in threshold images. Firstly the image is scanned, and if the object is found, the system outlines it by using selected tool, and then measures it. After measurement, the object becomes invisible, so the measurement can be performed on the next object. With this simplified procedure, and different protocol methods, it is easy to achieve wanted results, as shown in image 8 (Ferreira and Rasband, 2012).

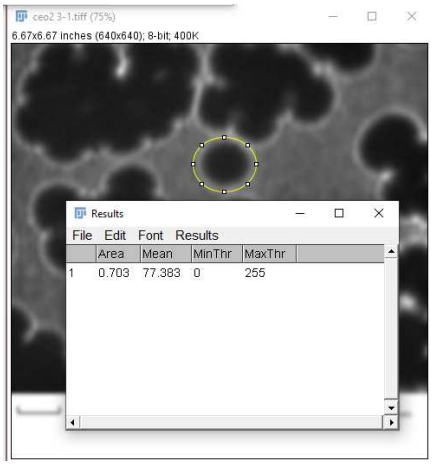

Image 8. The example of a single particle area measurement. By using this function, it is possible to measure the overall area of the particle, and then subtract the core of the particle, to know the thickness of the shell.

When using different protocol methods, there should always be the focus on the end result. Just a small adjustment can cause the difference in the image analyzes, and produce untrustworthy results.

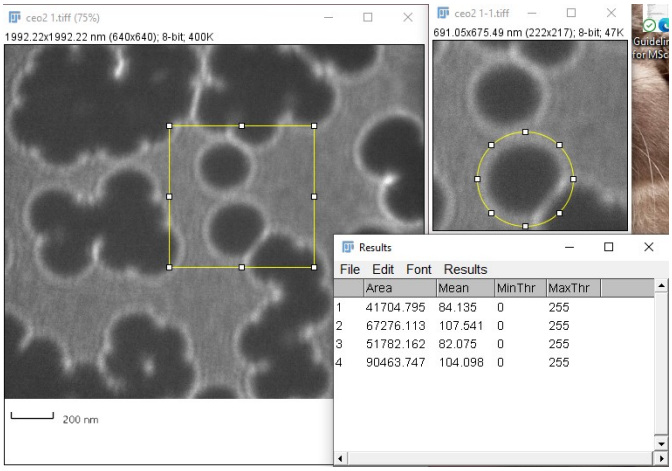

Image 9. The example of the shell thickness measurement procedure in ImageJ program. The area of interest is selected on the left side image, then the single particle is outlined to give the area in the table.

The procedure for analyzing the thickness of the shell for the CeO_2 Np`s within MSN is shown in the image 9. Selected area of interest was duplicated, and then the area of the core was measured, following with the area of the entire particle. The area of the core

was substituted from the area of entire NP, to get the area of the shell for the shell thickness calculation.

5 RESULTS

CeO_2 nanoparticles encapsulated with MSN were evaluated. Their composition and morphology were studied using TEM microscopy. Using ImageJ software, the nanoparticles in the TEM images were counted and their size was calculated, with the results showing the nanoparticles were uniform size (Image 10a). The measurement scale was adjusted to the desired scale before every image analysis, usually in nanometers. The final area of different particles was given in squared nanometers (nm^2) (Image 10b). It was possible to calculate the diameter of a single particle using the formula 1 for the area of a circle:

$$A = r^2\pi$$

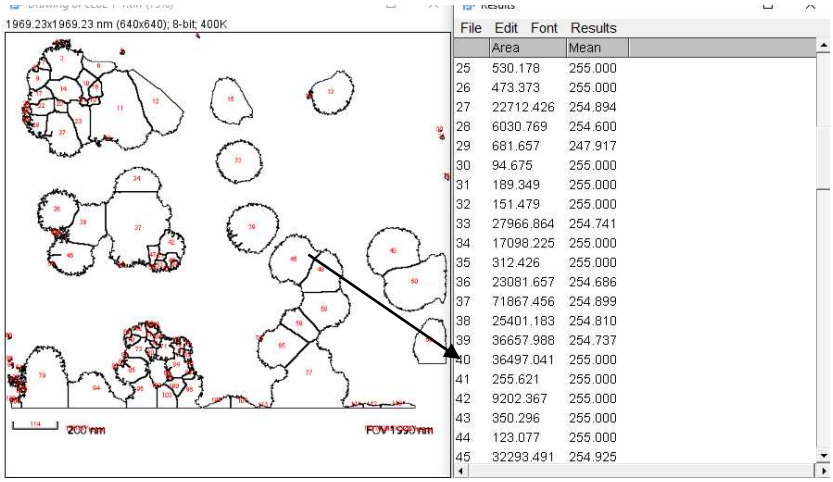

Image 10a An example of how to calculate the size of a single particle of CeO2 from the TEM image using ImageJ program. Desired particles are outlined and areas are measured in nm. The arrow points the particle area in the table, where each outlined particle contains the number corresponding the number in the table. The table in the right corner shows results of areas of selected particles.

As seen in Image 10a, image analysis was done using ImageJ in the following procedure: the particles are counted and outlined, then areas are calculated in the result table section in the right corner as shown with the arrow. This area was calculated using only particles with the uniform round shape. As an example, the area for the particle number 33 was calculated to be 27966.8 nm^2. The diameter was calculated from the formula 1, and was 94.4 nm.

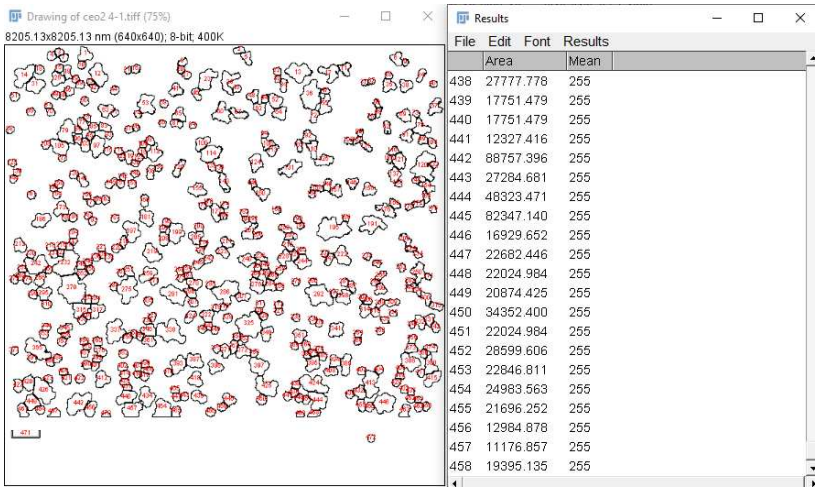

Image 10b The calculated area of 458 nanoparticles present at the TEM image using ImageJ. Every particle is counted with the final area calculation in nm^2.

From the processed TEM image presenting CeO_2 within MSN NP`s, there were 458 particles counted, numbered and outlined. The data window listed the area (in nm^2) for each particle. A summary of the particle count was transferred and saved in the Excel sheet. In the image, the average area was counted only from selected uniform round shape particles, and results are shown in the table 1.

Average area of CeO_2 within MSN in nm^2	Standard deviation in nm^2
30806.7	25901.5

Table 1. Final results of the average area of 458 CeO_2 within MSN nanoparticles in nm^2 and standard deviaton of the same results.

The average area of the CeO_2 at MSN nanoparticles from the image was calculated to be 30806.7 $nm^2 \pm$ 25901.5 (n=458). From the formula 1, the average radius value for the CeO_2 at MSN nanoparticles was calculated to be 99.03 nm.

The TEM images showed a clear separation of a core and a shell part of the single nanoparticle. In the ImageJ program, it was possible to calculate the shell thickens for the each CeO_2 at the MSN nanoparticle. The scale bar was set to nm and gave the length of each particle as shown with an arrow in the image 10c.

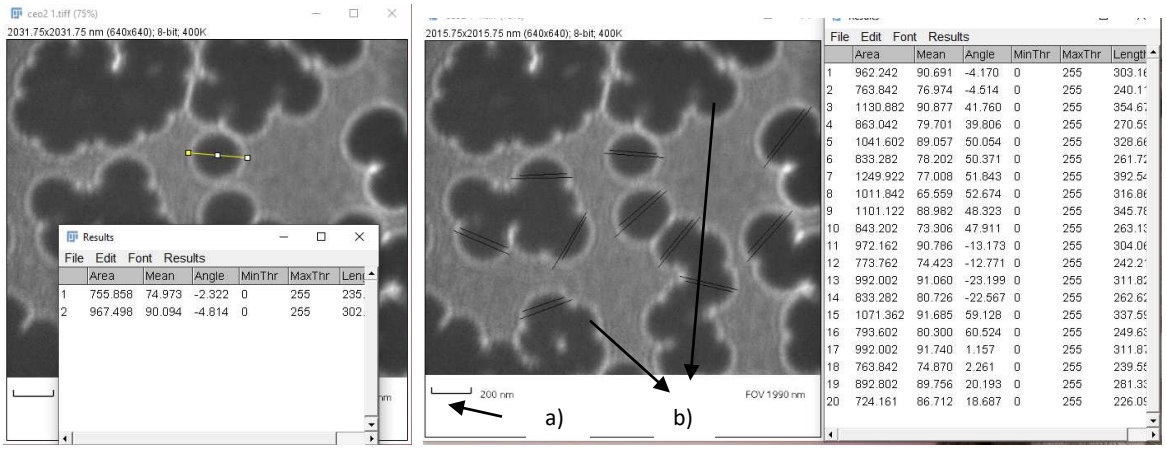

Image 10c Scale bar measurements for each particle (a), giving the length of the entire particle, as well as the shell of each particle (b). The length of the shell is subtracted from the length of the entire particle, giving the shell thickness length.

After the scale bar was set up to nm, the length of the entire particle was measured, followed by the length of core of the particle. The core length was distinguishable as it was visibly darker. The TEM images suggested a complete encapsulation of the core of nanoparticles. By subtracting the length of the length entire particle from the length of the core, the shell thickness was calculated. This procedure was repeated with 31 particles, then the mean value $\pm$ 12.3 (n=31) was calculated (Table 2).

Average shell thickness in nm	Number of particles tested	Standard deviation of average shell thickness
69.2	31	12.3

Table 2. The average result of the shell thickness for the CeO_2 at MSN nanoparticles. The core length was manually subtracted from the core+shell length for each nanoparticle. The result is given in nm calculated from 31 nanoparticles.

Figure 7 shows the average value for the shell thickness for 31 different nanoparticles used, and the result for the average shell thickness was 69.2 nm + 12.3 (n=31).

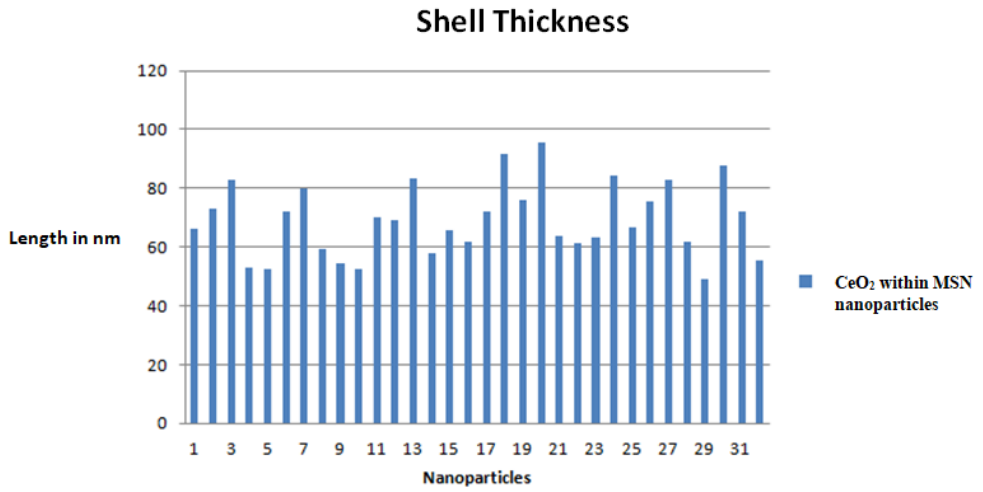

Figure 7. Chart presentation of the shell thickness of different 31 CeO_2 within MSN nanoparticles.

The average nanoparticle radius and average length of the shell thickness were measured in nm. The average core diameter length in nm was calculated by subtracting average shell thickness length from the average core diameter (radius multiplied by 2). If the average radius is 98.9 nm, then the diameter is 197.7 nm. When the average shell thickness length of 69.2 nm is subtracted, the core average diameter length is 128.5 nm (Figure 8).

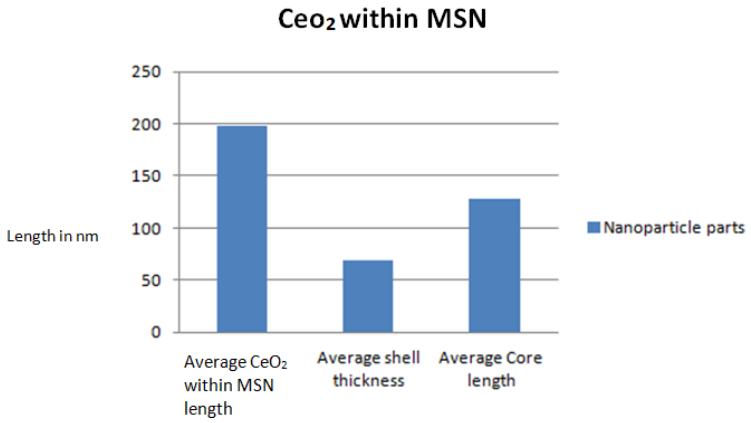

Figure 8. The chart comparing average length of the entire CeO_2 at MSN nanoparticle, average shell thickness, and Average core length of the 31 built particles.

The SEM images of the PEO-b-PFMA were analyzed in the ImageJ program (Image 11 a-f). Due to polymer dissolution, the only possible results were made from the assumption that little “craters” were particles, which got dissolved because of their position and shape in image 11e. The diameters of the craters were calculated manfully in the ImageJ program (Image 12).

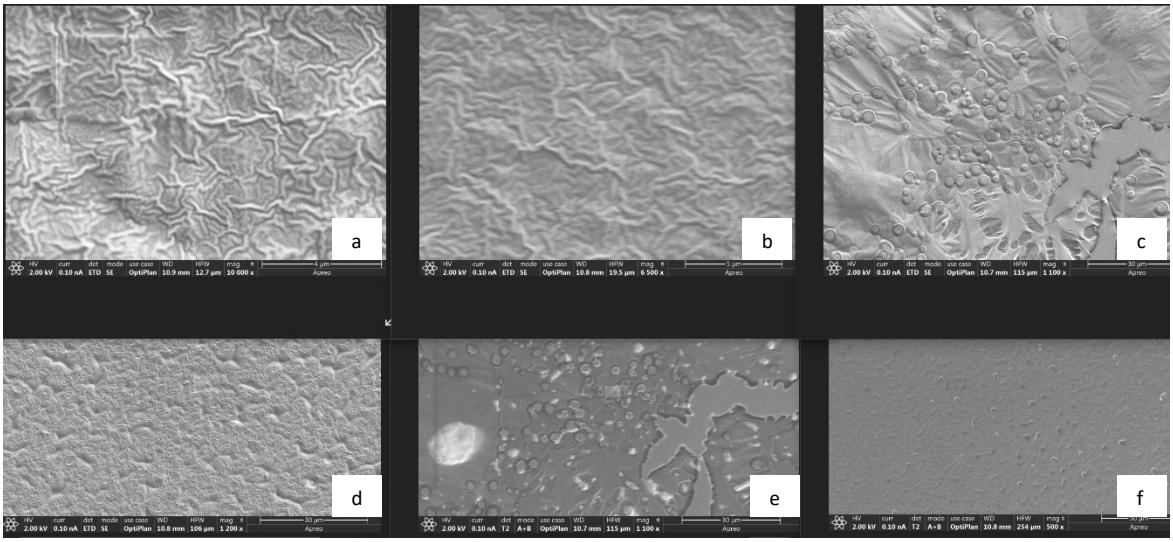

Image 11. Different dissolved PEO-b-PFMA. All images show PEO-b-PFMA synthesized using the same procedure.

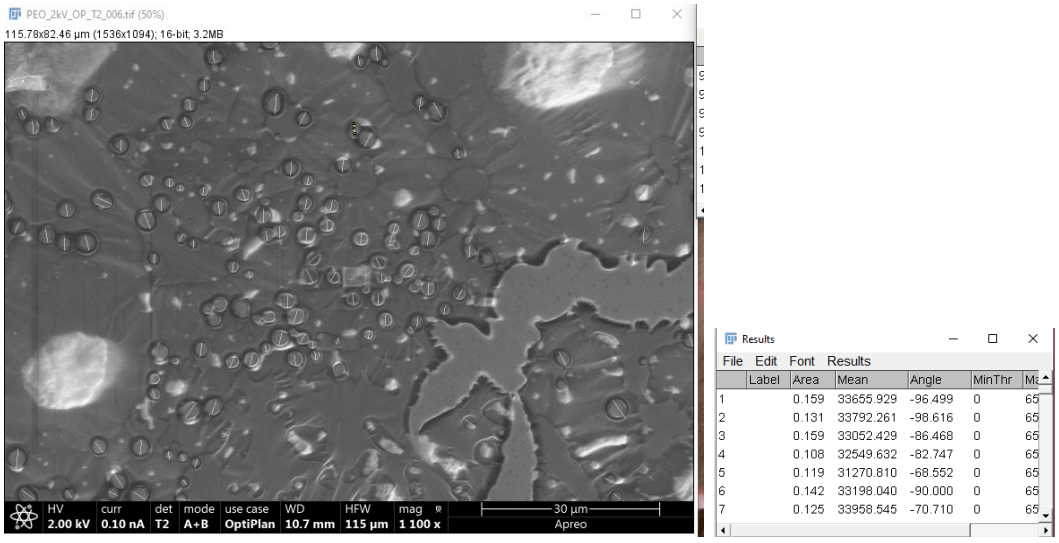

Image 12. The SEM image of the PEO-b-PFMA polymer, where the diameter (length) of craters (particles) was measured. The results are presented in the table.

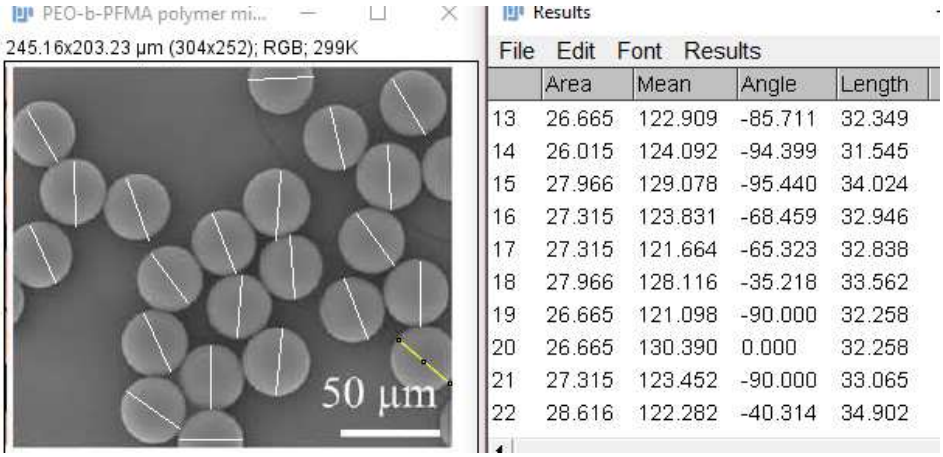

Image 13. The expected results of the PEO-b-PFMA particles. Microparticles supposed to be uniform size and shape. The measure scale was set up to 50 µm. It was possible to calculate the average area and length from the table with results.

SEM image analysis of the PEO-b-PFMA polymer was done using ImageJ. The final SEM images of the surface of the polymer showed that the particles fused together and were diluted because particles were not formed. The selected image 12 is showing little craters which are showing diluted particles. These craters have uniform shape, that's why it is assumed that they present single particle. The length of each crater was measured to calculate average size of the craters, as well as to try to validate whether the length of the craters matched the desired polymer length. The image measure scale was set to 50 µm. The results are shown in Image 13. The results were saved in the Excel sheet where the average length was calculated in µm. The average length was 1.9 µm $\pm$ 0.52 µm (n=102), while the average area was 0.15 µm $\pm$ 0.04 µm (n=102) (Table 3a). To validate whether these craters were indeed the dissolved polymer particles, the crater areas and lengths were compared to the expected areas and lengths of the polymer.

Average length in µm	Average area in µm
1.8	0.15

Table 3a. The table shows the calculations for the average area and length of the craters.

Average length in µm	Average area in µm
32.9	27.14

Table 3b. The expected results for the average area and length for the expected PEO-b-PFMA particles.

The average length is 32.9 µm +1.2 µm (n=22), while the average area is 27.14 µm + 0.97 µm (n=22).

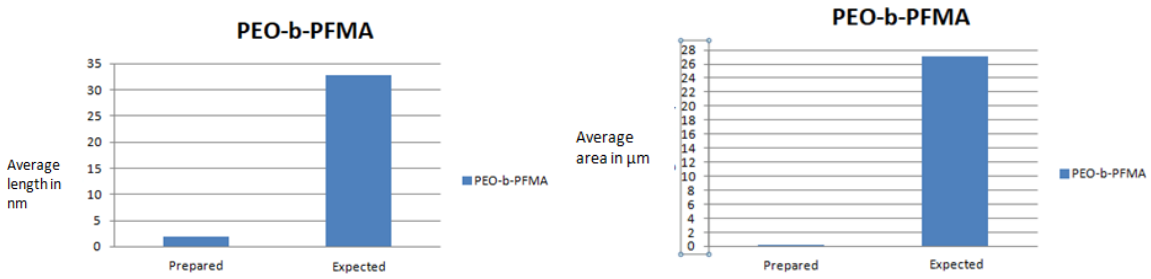

Figure 9. Two graphs, one with average length in µm for the expected and prepared PEO-b-PFMA, and another one for the average area in µm for the expected and prepared PEO-b-PFMA microparticles.

To confirm the assumption that craters are actually PEO-b-PFMA particles, t-Test for the length of the particles was necessary. Table 4 gives results of two-sample assuming equal variance t-Test.

Observations	Mean
102	1.9
22	32.9
P(T<=t) two tail	2E-153

Table 4. t-Test for length of PEO-b-PFMA. The number of particles prepared and analyzed was 102, where the number of the expected particles analyzed was 22.

While gold nanorods were not used in the project due to simplification, they were still synthesized. TEM images were used to determine the average length of nanorods. The desired size was planned to be between 100 and 200 nm, with the uniform appearance. The gold nanorods are shown with an arrow in the image 13a.

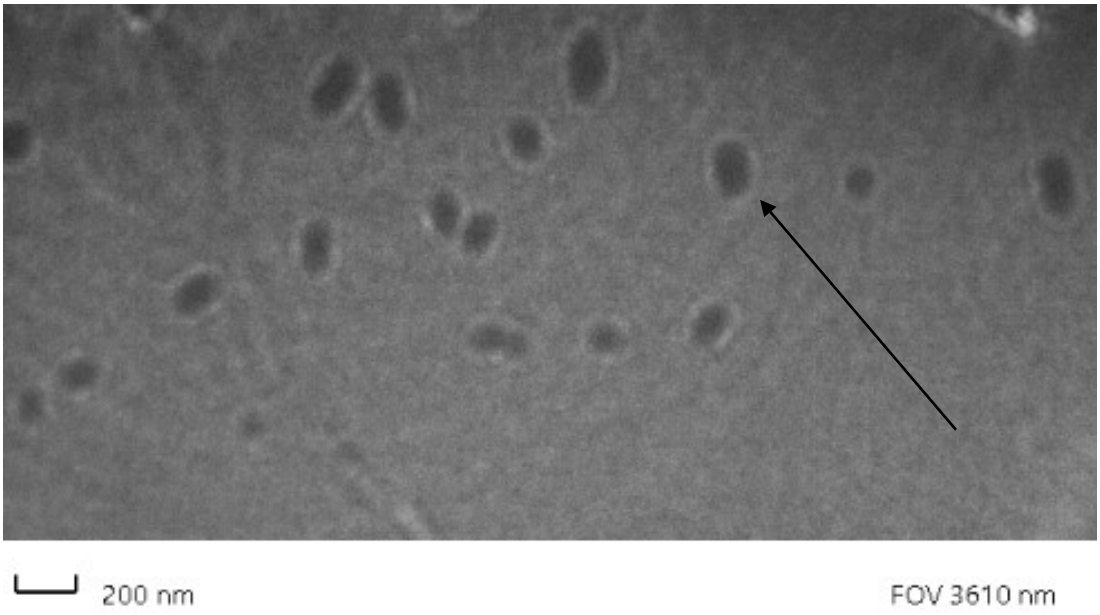

Image 13a. TEM images of gold nanorods built in the project procedure described in the synthesis of the Gold Nanorods.

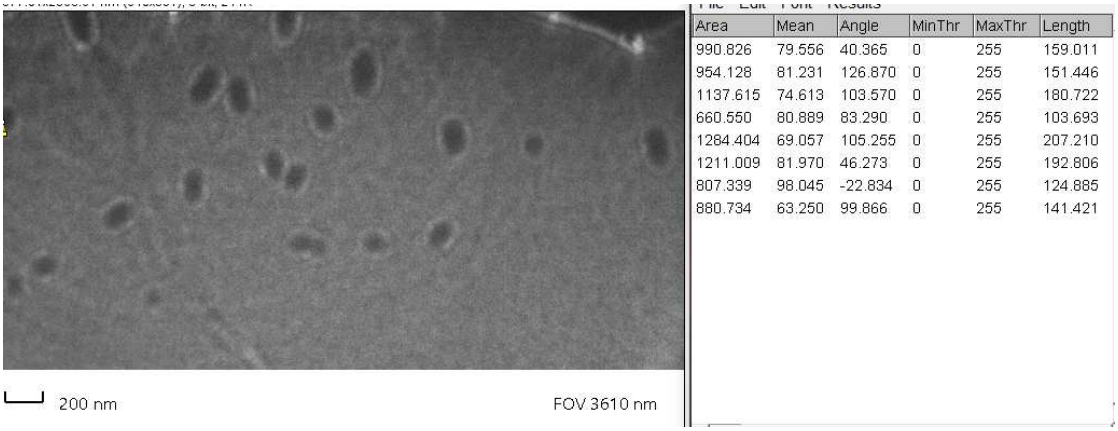

Area	Mean	Angle	MinThr	MaxThr	Length
990.826	79.556	40.365	0	255	159.011
954.128	81.231	126.870	0	255	151.446
1137.615	74.613	103.570	0	255	180.722
660.550	80.889	83.290	0	255	103.693
1284.404	69.057	105.255	0	255	207.210
1211.009	81.970	46.273	0	255	192.806
807.339	98.045	-22.834	0	255	124.885
880.734	63.250	99.866	0	255	141.421

Image 13b. Length measured of longitudinal part of the gold nanorods in Fiji program. The scale was set for 200 nm. In the table, different lengths are seen.

Average length in nm	Standard Deviation in nm
157.65	34.9

Table 5. Table with the calculation of the average length of the gold nanorods in nm. The length was compared between 8 nanorods, where the standard deviation was 34.87 nm

The project was stopped with the production of the PEO-b-PFMA microparticles necessary for the coating of all nanocomposites and required drugs. In the future research, the appropriate solvent is needed in order to avoid the dissolution and fusion of the polymer, following the coating of the nanocomposites and acquired drugs using microfluidics. Imaging of the microparticles after microfluidics is needed. Firstly, the imaging with the drug encapsulated within polymer, then, without the drug. With this technique, it is possible to test how much drug is needed in order for the targeted drug delivery system to be efficient.

6 DISCUSSION

The main focus of this project was to produce and test a drug delivery system to arthritic joints using lubricated microcompositions. The goal in the future is to treat osteoarthritis without surgical intervention. CeO_2 within MSN were perfect candidates of interest for the study because of their antioxidant properties and biocompatibility.

The two most important parameters regarding biocompatibility were size and surface of the particles. The core size was controlled to be from 50 nm, up to 300 nm, which was suitable for the endocytosis by the living cells. With the shell surrounding the core, the size was expected to be larger. The average diameter of the nanoparticles was around 197.7 nm $\pm$ 25901 nm^2 (n=458). While this average was around the goal size of 200 nm, the high standard deviation is a limitation, which could be caused by overlapping nanoparticles, as the ImageJ program maybe did not recognize multiple particles, and counted them as one, or possible human error.

Given the core-shell ratios calculated in the Results section, the assumption would be that the drug delivery system would have ability to arrive to targeted area at the certain time and release the drug in appropriate doses. Though this could not be done due to halting the project, another way to test the shell thickness would be by imaging the drug loaded particle, then imaging particles without the drug. This step is necessary in order to test if the corresponding shell thickness would release the adequate amount of drug needed for the treatment. If the drug is not released in desired amount, then the thickness is not meeting the goal and probably should be thinner.

In the process of the drug delivery, proper lubrication of microparticles was also an important factor to consider, as it is needed to protect the healthy tissue. In order for CeO_2 within MSN nanoparticles to have a lubricating effect, they were supposed to be coated in PEO-b-PFMA coating. This specific polymer coating was chosen as it has shown to have capability in drug delivery systems, as well as easy drug loading using microfluidics. As the drug delivery systems are under development and have a promising future, it is important to develop a biocompatible system. The goal was for the PEO-b-PFMA to release the drug under exposure of near-infrared light (NIR) with minimal or no damage to the body. Comparing the results from the figure 9, it is noticeable that the crater average area and the length average area are much smaller than the average area and length of the expected PEO-b-PFMA coating microparticles. The difference was assumed to be due to

dissolving PEO-b-PFMA microparticles. The assumption was that craters appeared on the areas where the particles used to obtain before the dissolving process. As the t-test showed significant difference in the crater and polymer sizes, this assumption was not correct. The craters could have occurred naturally as the polymer may not have been stable in storage conditions between the formation and the imaging. Additionally, the polymer imaged could have changed in composition. As there was no other way to prove whether the polymer was indeed the PEO-b-PFMA, there is also the chance that the polymer formed was different and therefore was not seen as the expected microparticles when imaged. Further tests will be needed to validate whether the craters observed are presenting particles and the proper polymer.

The project was stopped with the production of the polymer, because the polymer particles were not forming, they were diluted and fused together. There were difficulties in finding the appropriate storage solvent while finalizing the last step with the polymer coating of the particles. The SEM images 11a-11f are the proof that the polymer built nanoparticles were dissolved. This could have been due to one of the storage solvents. Another time-consuming step was finding the right optimization for forming the droplets of the PEO-b-PFMA coating. By trying many different methods, the appropriate optimization was not found.

Gold nanorods were prepared, as they contain suitable optical properties and have successful applications in the diagnosis of osteoarthritis and its treatment. The length of the particles was around 157.6 nm, between the desired length. They are widely used, with applications in thermal therapy, bioimaging, and drug delivery, which made them a perfect candidate in this project. But, to simplify the project, built gold nanorods were not used.

Given the unforeseen circumstances due to the coronavirus pandemic, the project was adjusted and simplified, so the drug was not used. It is still of interest to use this drug in future research in order to increase the bone formation and to use miRNA874 as a therapeutic intervention for osteoarthritis.

Furthermore, collagen IgG_2 was not introduced to the microcompositions built for the drug delivery, as it was originally planned. The goal for the future research would be to attach collagen IgG_2 to CeO_2 within MSN nanoparticles to form an antibody-antigen binding to collagen type II in joints and joint fluids. The major role of collagen IgG_2 would be to reduce symptoms of osteoarthritis by stimulating collagen production in joints.

The 5-ASA drug supposed to be inserted within PEO-b-PFMA microparticles. This step would conclude the experiment building particles. Because the polymer could not be formed, the drug was not added. In the future experiments, when adding 5-ASA, it is important to consider several things. Firstly, it is important to test and decide how much drug is necessary in single CeO_2 particle. Secondly, it is necessary to decide the percentage of the drug in the final system. It is always good to start with the higher amount of the drug, and lower it down in the case it is needed. If there is not an exact amount of the drug in the microparticles, the drug delivery system would not be functional. The TEM imaging is necessary before and after the drug insertion to decide if the experiment was successful.

Once the project is finalized, it could be tested in animals. If successful, the next step would be clinical studies.

7 CONCLUSION

Due to the unforeseen halting of the experiment, much of the proposed project was not completed. Despite this, the physical appearance of CeO_2 within MSN seems promising. The particles were of uniform size, however, the high standard deviation value within the particle size requires further investigation to determine whether the nanoparticles fit the initial desired criteria for the drug delivery system.

The biggest challenge in the project was connected with the synthesis of the PEO-b-PFMA coating. Once the optimization for forming droplets was done, the droplets would dissolve within 24 hours of formation. Further research must be done to determine optimal storage solutions in order to keep the droplets stable so that they may be used to finalize the drug delivery system.

As the project was halted, the hypothesis remains that this drug delivery system, with the chosen drugs, can be developed with the hopes of one day being used clinically and helping millions of people suffering from osteoarthritis.

8 ACKNOWLEDGES

I would like to thank Associate Prof. Hongbo Zhang, as well his entire Precision Nanomedicine and Diagnostics laboratory team. Also, I would like to thank PhD. Jixiang Wang for supervision at the beginning of the thesis project. Thanks to Prof. Sergey Filippov for the useful advices. Special thanks to my Biomedical Imaging program supervisors Diana Toivola and Joanna Pylvänäinen, as well as other BIMA professors and classmates.

9 REFERENCES

Abdu Allah, H.H., and A.N. A El Shorbagi. 2016. 5-Aminosalyclic Acid (5-ASA): A Unique Anti-Inflammatory Salicylate. *Med. Chem. (Los. Angeles).* 06. doi:10.4172/2161-0444.1000361.

Al-snafi, A.E. 2014. International Journal for Pharmaceutical Research Scholars (IJPRS). 671–677.

Arvizo, R., R. Bhattacharya, and P. Mukherjee. 2010. Gold nanoparticles: Opportunities and challenges in nanomedicine. *Expert Opin. Drug Deliv.* 7:753–763. doi:10.1517/17425241003777010.

Askelof, E., and S. Helander. 1992. Mechanism of action of 5-arninosalicylic acid. 1992:151–165.

Beebe, D.J., G.A. Mensing, and G.M. Walker. 2002. Physics and applications of microfluidics in biology. *Annu. Rev. Biomed. Eng.* 4:261–286. doi:10.1146/annurev.bioeng.4.112601.125916.

Blagojevic, M., C. Jinks, A. Jeffery, and K.P. Jordan. 2010. Risk factors for onset of osteoarthritis of the knee in older adults: a systematic review and meta-analysis. *Osteoarthr. Cartil.* 18:24–33. doi:10.1016/j.joca.2009.08.010.

Catalanotto, C., C. Cogoni, and G. Zardo. 2016. MicroRNA in control of gene expression: An overview of nuclear functions. *Int. J. Mol. Sci.* 17. doi:10.3390/ijms17101712.

Cooper, D.L., C.M. Conder, and S. Harirforoosh. 2014. Nanoparticles in drug delivery: Mechanism of action, formulation and clinical application towards reduction in drug-associated nephrotoxicity. *Expert Opin. Drug Deliv.* 11:1661–1680. doi:10.1517/17425247.2014.938046.

Cui, P., and S. Wang. 2019. Application of microfluidic chip technology in pharmaceutical analysis: A review. *J. Pharm. Anal.* 9:238–247. doi:10.1016/j.jpha.2018.12.001.

Douroumis, D., I. Onyesom, M. Maniruzzaman, and J. Mitchell. 2013. Mesoporous silica nanoparticles in nanotechnology. *Crit. Rev. Biotechnol.* 33:229–245. doi:10.3109/07388551.2012.685860.

El-Dairi, M., and R.J. House. 2019. Optic nerve hypoplasia. *Handb. Pediatr. Retin. OCT Eye-Brain Connect.* 285–287. doi:10.1016/B978-0-323-60984-5.00062-7.

Ferreira, T., and W. Rasband. 2012. ImageJ User Guide User Guide ImageJ. *Image J user Guid.* 1.46r. doi:10.1038/nmeth.2019.

Galogahi, F.M., Y. Zhu, H. An, and N.T. Nguyen. 2020. Core-shell microparticles: Generation approaches and applications. *J. Sci. Adv. Mater. Devices*. 5:417–435. doi:10.1016/j.jsamd.2020.09.001.

Goodhew, P.J. 2011. General Introduction to Transmission Electron Microscopy TEM. *Aberration-Corrected Anal. Transm. Electron Microsc.* 1–19. doi:10.1002/9781119978848.ch1.

Grässel, S., and D. Muschter. 2020. Recent advances in the treatment of osteoarthritis [version 1 ; peer review : 3 approved]. *F1000Research*. 9:1–17.

Haine, A.T., and T. Niidome. 2017. Gold nanorods as nanodevices for bioimaging, photothermal therapeutics, and drug delivery. *Chem. Pharm. Bull.* 65:625–628. doi:10.1248/cpb.c17-00102.

Han, H. 2016. Nnm-11-673.Pdf. 11:673–692.

Hayes, R., A. Ahmed, T. Edge, and H. Zhang. 2014. Core-shell particles: Preparation, fundamentals and applications in high performance liquid chromatography. *J. Chromatogr. A*. 1357:36–52. doi:10.1016/j.chroma.2014.05.010.

He, D., S. Wang, L. Lei, Z. Hou, P. Shang, X. He, and H. Nie. 2015. Core-shell particles for controllable release of drug. *Chem. Eng. Sci.* 125:108–120. doi:10.1016/j.ces.2014.08.007.

Hosseini, M., and M. Mozafari. 2020. Cerium oxide nanoparticles: Recent advances in tissue engineerings. *Materials (Basel).* 13:1–46. doi:10.3390/ma13143072.

Huang, X., S. Neretina, and M.A. El-Sayed. 2009. Gold nanorods: From synthesis and properties to biological and biomedical applications. *Adv. Mater.* 21:4880–4910. doi:10.1002/adma.200802789.

Hunter, D.J., and F. Eckstein. 2009. Exercise and osteoarthritis. *J. Anat.* 214:197–207. doi:10.1111/j.1469-7580.2008.01013.x.

Jafari, S., H. Derakhshankhah, L. Alaei, A. Fattahi, B.S. Varnamkhasti, and A.A. Saboury. 2019. Mesoporous silica nanoparticles for therapeutic/diagnostic applications. *Biomed. Pharmacother.* 109:1100–1111. doi:10.1016/j.biopha.2018.10.167.

Jixiang Wang. 2019. Core&Core-shell PROTOCOL.

Jokinen, V. 2017. MT-0.6081 Microfluidics and BioMEMS, Basics, Laminar flow, shear and flow profiles. 11–15.

De Jong, W.H., and P.J.A. Borm. 2008. Drug delivery and nanoparticles: Applications and

hazards. *Int. J. Nanomedicine*. 3:133–149. doi:10.2147/ijn.s596.

Liechty, W.B., D.R. Kryscio, B. V. Slaughter, and N.A. Peppas. 2010. Polymers for drug delivery systems. *Annu. Rev. Chem. Biomol. Eng.* 1:149–173. doi:10.1146/annurev-chembioeng-073009-100847.

Loscalzo, D.E.H.R.C.J. 2011. 基因的改变NIH Public Access. *Bone*. 23:1–7. doi:10.1002/art.34453.Osteoarthritis.

Mackie, E.J., Y.A. Ahmed, L. Tatarczuch, K.S. Chen, and M. Mirams. 2008. Endochondral ossification: How cartilage is converted into bone in the developing skeleton. *Int. J. Biochem. Cell Biol.* 40:46–62. doi:10.1016/j.biocel.2007.06.009.

Mazetyte-Stasinskiene, R., and J.M. Köhler. 2020. Sensor micro and nanoparticles for microfluidic application. *Appl. Sci.* 10:1–37. doi:10.3390/app10238353.

Mohanraj, V.J., and Y. Chen. 2006. Nanoparticles-A Review. 5. 561–573 pp.

Mora, J.C., R. Przkora, and Y. Cruz-Almeida. 2018a. Knee osteoarthritis: Pathophysiology and current treatment modalities. *J. Pain Res.* 11:2189–2196. doi:10.2147/JPR.S154002.

Mora, J.C., R. Przkora, and Y. Cruz-Almeida. 2018b. Knee osteoarthritis: pathophysiology and current treatment modalities. *J. Pain Res.* Volume 11:2189–2196. doi:10.2147/JPR.S154002.

Naumann, A., J.E. Dennis, A. Awadallah, D.A. Carrino, J.M. Mansour, E. Kastenbauer, and A.I. Caplan. 2002. Immunochemical and mechanical characterization of cartilage subtypes in rabbit. *J. Histochem. Cytochem.* 50:1049–1058. doi:10.1177/002215540205000807.

One Digital Drive. 2018. P-30. 11.

Peppas, N.A., and B. Narasimhan. 2014. Mathematical models in drug delivery: How modeling has shaped the way we design new drug delivery systems. *J. Control. Release*. doi:10.1016/j.jconrel.2014.06.041.

Perrotta, C., P. Pellegrino, E. Moroni, C. De Palma, D. Cervia, P. Danelli, and E. Clementi. 2015. Five-aminosalicylic acid: An update for the reappraisal of an old drug. *Gastroenterol. Res. Pract.* 2015. doi:10.1155/2015/456895.

Salma, S.A., M.P. Patil, D.W. Kim, C.M.Q. Le, B.H. Ahn, G. Do Kim, and K.T. Lim. 2018. Near-infrared light-responsive, diselenide containing core-cross-linked micelles prepared by the Diels-Alder click reaction for photocontrollable drug release

application. *Polym. Chem.* 9:4813–4823. doi:10.1039/c8py00961a.

Scarabelli, L., A. Sánchez-Iglesias, J. Pérez-Juste, and L.M. Liz-Marzán. 2015. A "Tips and Tricks" Practical Guide to the Synthesis of Gold Nanorods. *J. Phys. Chem. Lett.* 6:4270–4279. doi:10.1021/acs.jpclett.5b02123.

Singh, R., and J.W. Lillard. 2009. Nanoparticle-based targeted drug delivery. *Exp. Mol. Pathol.* 86:215–223. doi:10.1016/j.yexmp.2008.12.004.

Snp, A., and C. Reagent. High Speed Digital Isolator. 1–2.

Sun, X., H. Zhang, L. Zhang, X. Wang, and Q.F. Zhou. 2005. Synthesis of amphiphilic poly(ethylene oxide)-b-poly(methyl methacrylate) diblock copolymers via atom transfer radical polymerization utilizing halide exchange technique. *Polym. J.* 37:102–108. doi:10.1295/polymj.37.102.

Umlauf, D., S. Frank, T. Pap, and J. Bertrand. 2010. Cartilage biology, pathology, and repair. *Cell. Mol. Life Sci.* 67:4197–4211. doi:10.1007/s00018-010-0498-0.

Wang, Y., R.N. Dave, and R. Pfeffer. 2004. Polymer coating/encapsulation of nanoparticles using a supercritical anti-solvent process. *J. Supercrit. Fluids*. 28:85–99. doi:10.1016/S0896-8446(03)00011-1.

Weiss, A.D. 1983. Scanning Electron Microscopes. *Semicond. Int.* 6:90–94. doi:10.1016/s0026-0576(03)90123-1.

Wittenauer, R., L. Smith, and K. Aden. 2013. Priority Medicines for Europe and the World " A Public Health Approach to Innovation " Update on 2004 Background Paper Background Paper 6 . 12 Osteoarthritis. 1–31.

World Health Organization. 2013. Essential medicines and health products - Priority diseases and reasons for inclusion - Osteoarthritis. *World Heal. Organ.* 12:6–8.

Xu, C.T., S.Y. Meng, and B.R. Pan. 2004. Drug therapy for ulcerative colitis. *World J. Gastroenterol.* 10:2311–2317. doi:10.3748/wjg.v10.i16.2311.

Zhang, D., L. Men, and Q. Chen. 2011. Microfabrication and applications of opto-microfluidic sensors. *Sensors*. 11:5360–5382. doi:10.3390/s110505360.

Zhao, Q., D. Yuan, J. Zhang, and W. Li. 2020. A review of secondary flow in inertial microfluidics. *Micromachines*. 11:1–23. doi:10.3390/MI11050461.

Zhou, Y., G. Quan, Q. Wu, X. Zhang, B. Niu, B. Wu, Y. Huang, X. Pan, and C. Wu. 2018. Mesoporous silica nanoparticles for drug and gene delivery. *Acta Pharm. Sin. B*. 8:165–177. doi:10.1016/j.apsb.2018.01.007.